Kansas State University

Manhattan, Kansas 66502

Engineering Experiment Station
Seaton Hall

October 11, 1966

National Aeronautics and
Space Administration
Washington, D. C. 20546

Ref: Nc-NsG-692/17-01-005

Gentlemen:

We are pleased to transmit herewith the semi-annual status report for the National Aeronautics and Space Administration Grant referred to above. The report covers the period of March 1, 1966 to August 31, 1966.

The research projects included in this report are as follows:

1. The Measurement of Lunar and Planetary Infrared Radiation	Dr. E. Brock Dale	Physics
2. Mitochondrial Heat Production	Dr. R. K. Burkhard	Biochemistry
3. Analytical Studies in the Learning and Memory of Skilled Performance	Dr. Merrill E. Noble	Psychology
4. Optimization of Space System Design	Dr. Frank A. Tillman	Industrial Eng.
5. Experiments with Ultraviolet Light	Dr. Charles Mandeville	Physics
6. Tracks of Heavy Ions in Emulsion	Dr. Robert Katz	Physics
7. Ideal Single Side Band Modulation and Demodulation	Dr. Charles Halijak	Electrical Eng.
8. Determination of Optimum Nozzle Contours for the Expansion of Dissociated Gases by Methods of the Variational Calculus	Dr. James E. Bowyer	Mechanical Eng.

We will appreciate receiving comments or suggestions from any of those who review this report.

Sincerely yours,

RESEARCH COORDINATING COUNCIL

John Lott Brown, Chairman
Vice-President

A. B. Cardwell, Director
Bureau of General Research

Floyd Smith, Director
Agriculture Experiment Station

Leland S. Hobson, Director
Engineering Experiment Station
Secretary

Leland S. Hobson

sm

Enclosures

NATIONAL AERONAUTICS AND SPACE
ADMINISTRATION NsG-692

THE MEASUREMENT OF LUNAR AND PLANETARY INFRARED RADIATION

Department of Physics
E. Brock Dale, Principal Investigator

During the six month period just past the detector-photometer system has been completely redesigned and rebuilt. The major changes include: (1) improved mechanical stability in all components, (2) incorporation of additional low-temperature baffles into the detector housing, (3) improved electrical contact to the detector, (4) an increase in detector size so that, by interchanging masks, we can adapt the photometer to measurement of total radiation from the planets, (5) incorporation of a 1 liter/sec ion pump to evacuate the system continuously while it is in use.

The latter was found to be a necessity because of cyropumping and resulting condensation on the 20^{0}K cold finger and the detector. The elimination of leaks from the system has been a serious problem because of the small pump capacity. Consideration of weight precludes the use of a larger pump. With the present system we are able to maintain a vacuum of 10^{-5} torr. There are no leaks greater than 10^{-10} liter atmospheres/sec, indicating that the gas load is primarily due to outgassing. Since this will be eliminated at low temperature, we expect no further difficulty.

Alterations yet to be made are: (1) incorporation of a tracking camera that will photograph the object under surveillance projected onto a reference reticle, (2) elimination of heat transfer between the rotating shutter and the shutter drive motor.

A study of conditions affecting the noise equivalent power (NEP) of

photoconductive detectors has been carried out. Some errors and omissions have been found in the open literature. Our results will be published in due course.

Semi-annual Report

for

NASA Project N2G-692

"Mitochondrial Heat Production"

prepared by

R.K. Burkhard, Principal Investigator

September 22, 1966

Research Performed

The construction of a calorimeter suitable for the measurement of heat produced by mitochondria has been started. The machining of a heat sink is currently being done in the Department of Industrial Engineering. The construction of glass reaction vessels to go into the heat sink is being done in the Department of Physics. The construction of the thermopile which will surround the reaction vessel and measure heat flow to the heat sink is being constructed in our own laboratory. Experimentation with mitochondria will need to await completion of the microcalorimeter.

Publications

G.L. Dohm, "The Effect of Centrifugal Fields on Enzymatic Reactions", M.S. thesis, 1966, Kansas State University.

Semi-Annual Report
NASA Grant NsG 692
March 1, 1966 - August 31, 1966
Analytical Studies in the Learning and Memory
of Skilled Performance

Merrill E. Noble, Richard E. Christ, and Stephen J. Handel

During the six month period ending August 31, 1966, data were collected on an additional psychophysical study of the ability to perceive the coincidence between forms presented to the peripheral retina. Four forms, triangles, inverted triangles, V's, and inverted V's were employed, since earlier data collected in connection with this research grant suggested that triangles were perceived more accurately than open triangles (V's). These data, together with other data and theories in the field of visual perception led to the study just completed. Analyses of those data are now under way.

Drs. Richard E. Christ and Stephen J. Handel, and Merrill E. Noble acted as co-investigators during much of the past six months, and will continue to do so in the new investigations now in progress.

Merrill E. Noble
Merrill E. Noble
Principal Investigator

bd

Project: National Aeronautics and Space Administration NsG-692

Title: Optimization of Space Systems Design

Department: Industrial Engineering Department

Investigator: Dr. Frank A. Tillman, Head

The original investigator on this phase of the project, Dr. George F. Schrader, has left Kansas State University. Dr. Tillman took over and continued the work on the same topic. The following are the principle areas investigated:

1. OPTIMUM SOLUTION OF A STOCHASTIC INVENTORY PROBLEM BY THE DISCRETE MAXIMUM PRINCIPLE

   This effort illustrates that the discrete maximum principle can be applied to problems of probabilistic nature. A multistage inventory model with uncertain demands is solved for the optimum level of starting inventory which minimizes the costs. The optimal sequence of inventory levels of the multistage inventory model is found by using two recurrence equations.

2. OPTIMIZATION OF SYSTEMS RELIABILITY

   The purpose of this effort is to obtain an optimum redundancy of the parallel system by the discrete maximum principle. The objective function is to maximize the system profit. A simple computational procedure has been obtained for the optimum design of the multistage parallel systems by this method. Two numerical examples have been worked out in detail.

3. THE APPLICATION OF THE DISCRETE MAXIMUM PRINCIPLE TO TRANSPORTATION PROBLEMS WITH LINEAR AND NON-LINEAR COST FUNCTIONS

   Optimization of transportation problems with only one type of resource and with the equal total supply and total demand is carried out by means of a discrete

version of the maximum principle. A general algorithm derived from the discrete version of the maximum principle and formulation of the transportation problem in terms of this algorithm are outlined. A simple problem involving a linear cost function and with three depots is systematically analysed in order to obtain a generalized computational procedure for solving the problem with more than three depots. The use of this procedure is illustrated by solving a problem with four depots. Problems involving non-linear cost functions and having two and three depots are also considered.

Annual Report of the Work

of

NASA Grant NsG-$6_9$2

Experiments with Ultraviolet Light

Principal Investigator: C. E. Mandeville

Department of Physics
Kansas State University
Manhattan, Kansas

1 September 1966

I. INTRODUCTION

In the last annual report, a general discussion was given to describe the nature of the effect under study. Both ultraviolet and visible light are generated when the relative motion of mercury and glass occurs. In the previous report some preliminary results were given, and the first form of apparatus for photon detection was described. Briefly, it can be said that a glass ball containing liquid mercury, mercury vapor, and helium gas, is rotated at various values of rpm.

In a brief semi-annual report of date 24 March 1966, improvement of the apparatus over that of the previous year was discussed. Experiments have continued with the use of photomultipliers as detectors rather than the photosensitive Geiger counters with which the measurements were initially commenced.

All following discussions and related figures concerns a glass ball which contained a few grains of mercury and helium at pressure 0.6 mm Hg. Measurements were performed at room temperature. The ball itself was made of Corning 9741 glass which transmits not only the visible but the ultraviolet as well.

II. NEW MEASUREMENTS

A. The "Time Effect"

In the course of earlier studies it had been noted that the light yield from the rotating glass ball containing mercury had a tendency to decrease during the time of protracted rotation; that is, during a long period of continuous running, the intensity of emission decreased markedly.

Using an essentially solar blind RCA-C-70128 ultraviolet sensitive photomultiplier tube as detector, the data of Fig. 1 were obtained. The decrease in intensity of photon emission as the running time increases is

clearly evident. At this point, it should also be mentioned that the use of photomultiplier tubes as detectors also revealed the pulsed nature of the emission. When viewed on an oscilloscope, the light emission appeared to have a rise time of 2 microseconds. The decay time was artificially lengthened by the time constant of the associated circuitry. From the rise time, it can be estimated, of course, that the full width in time at half maximum of the pulse is one microsecond.

The explanation for the decrease of yield with time of continuous rotation has not been determined. A related curve obtained with use of a photosensitive Geiger counter is shown in Fig. 2.

B. Pulse Height as a Function of Rotation Rate.

Figs. 3 through 8 demonstrate the behavior of the distribution of pulse heights associated with emission obtained from the ball. It will be noted that the average pulse height increases to a certain point, ultimately decreasing as the velocity of rotation is further increased. Explanatory captions are given for each figure. The reason for decrease of emission of the light at the higher rotation rates is not known yet but is thought to be related to the transit time of the electrons, the time for electrons to move from mercury to glass.

Time Effect Run

.6 mm Hg base
7012-8 P.M. AT 1.5KVDC
MAY 1966

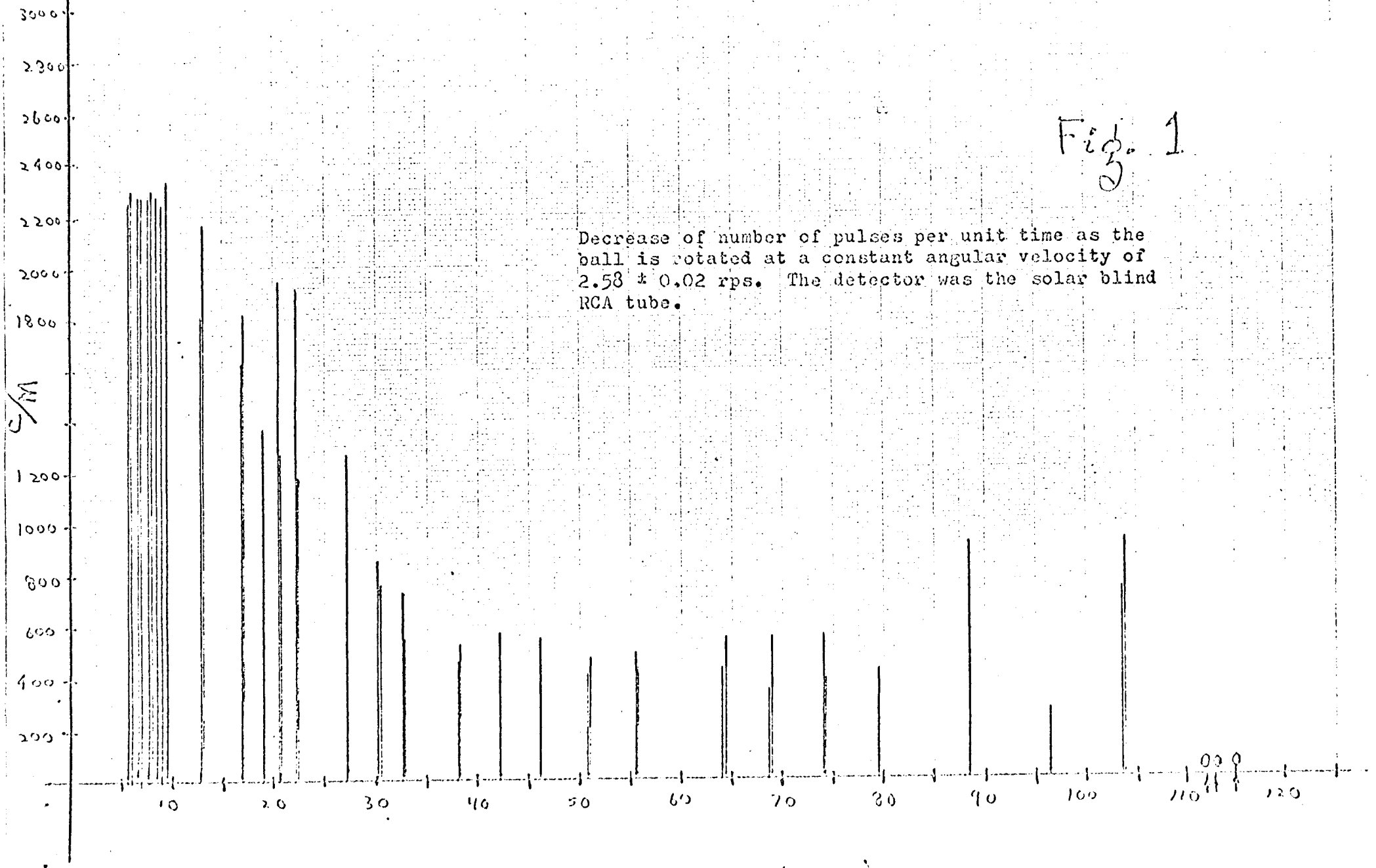

Fig. 1

Decrease of number of pulses per unit time as the ball is rotated at a constant angular velocity of 2.58 ± 0.02 rps. The detector was the solar blind RCA tube.

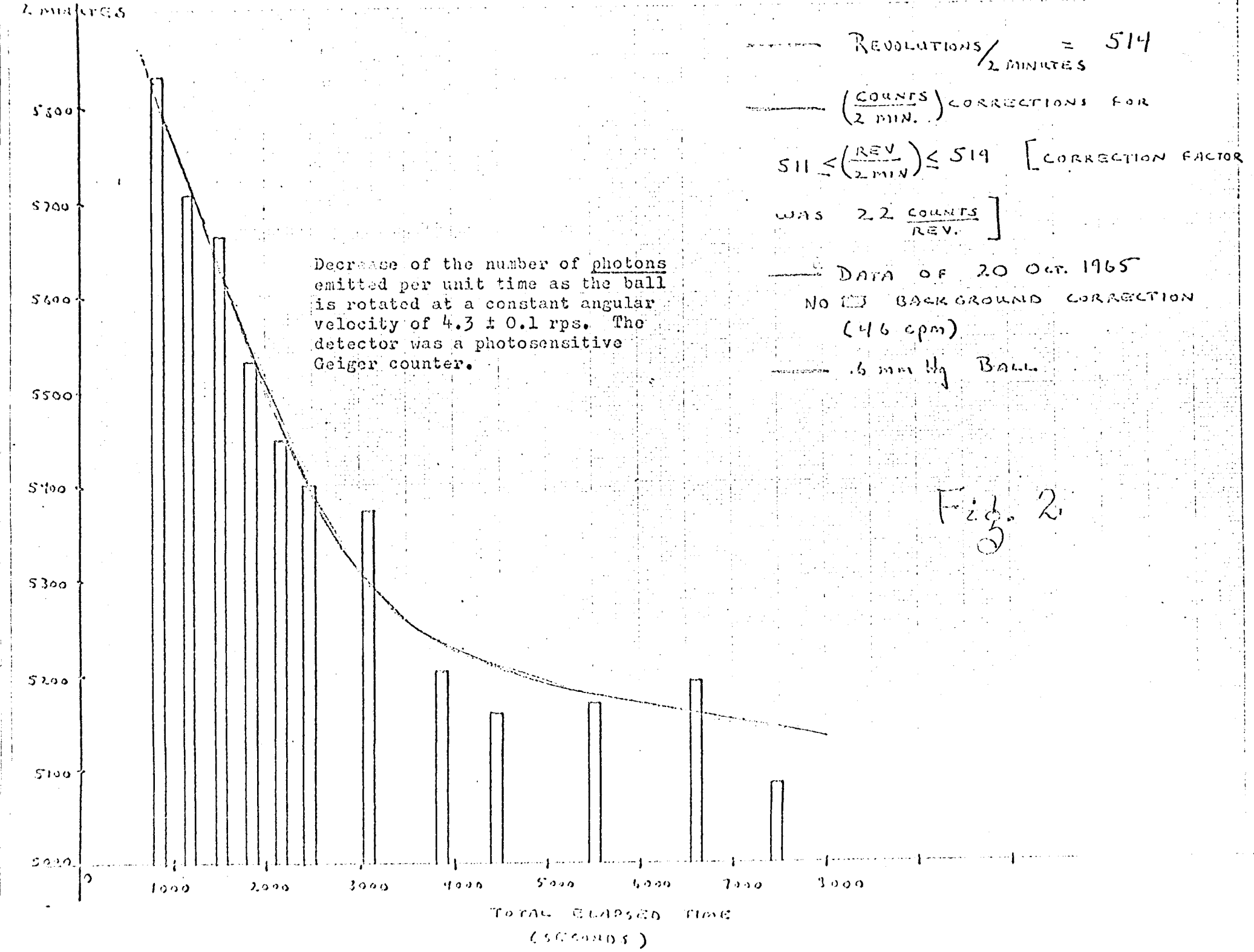
2 minutes
5800
5700
5600
5500
5400
5300
5200
5100
5000
0
1000
2000
3000
4000
5000
6000
7000
8000
Total elapsed time
(seconds)
Revolutions/2 minutes = 514
(Counts/2 min.) corrections for
511 ≤ (Rev/2 min) ≤ 519 [correction factor
was 2.2 counts/rev.]
Data of 20 Oct. 1965
No background correction
(46 cpm)
.6 mm Hg Ball
Decrease of the number of photons emitted per unit time as the ball is rotated at a constant angular velocity of 4.3 ± 0.1 rps. The detector was a photosensitive Geiger counter.

Fig. 2.

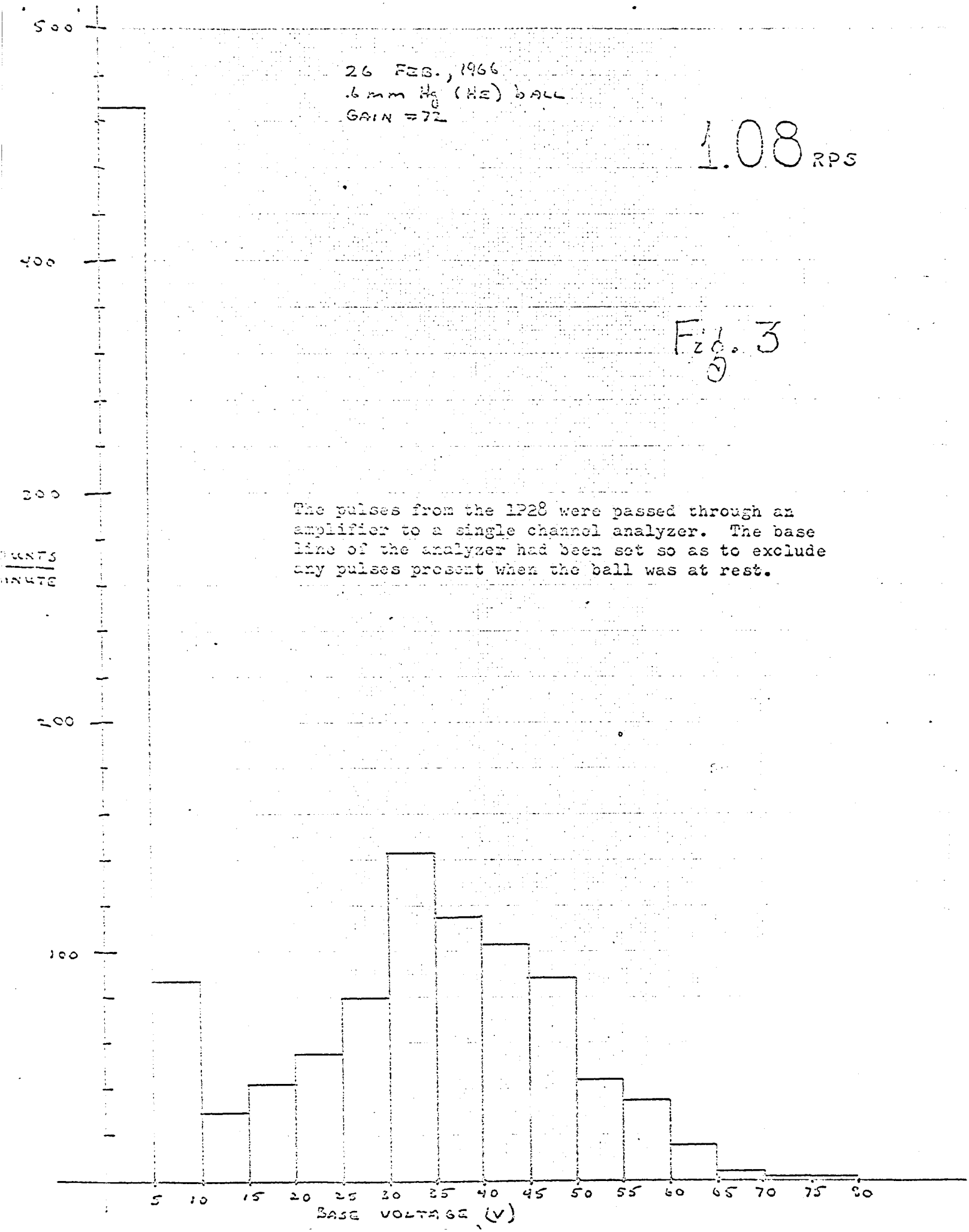
26 FEB., 1966
.6 mm Hg (He) BALL
GAIN = 72
1.08 RPS
Fig. 3
The pulses from the 1P28 were passed through an amplifier to a single channel analyzer. The base line of the analyzer had been set so as to exclude any pulses present when the ball was at rest.
500
400
300
200
100
COUNTS PER MINUTE
5 10 15 20 25 30 35 40 45 50 55 60 65 70 75 80
BASE VOLTAGE (V)

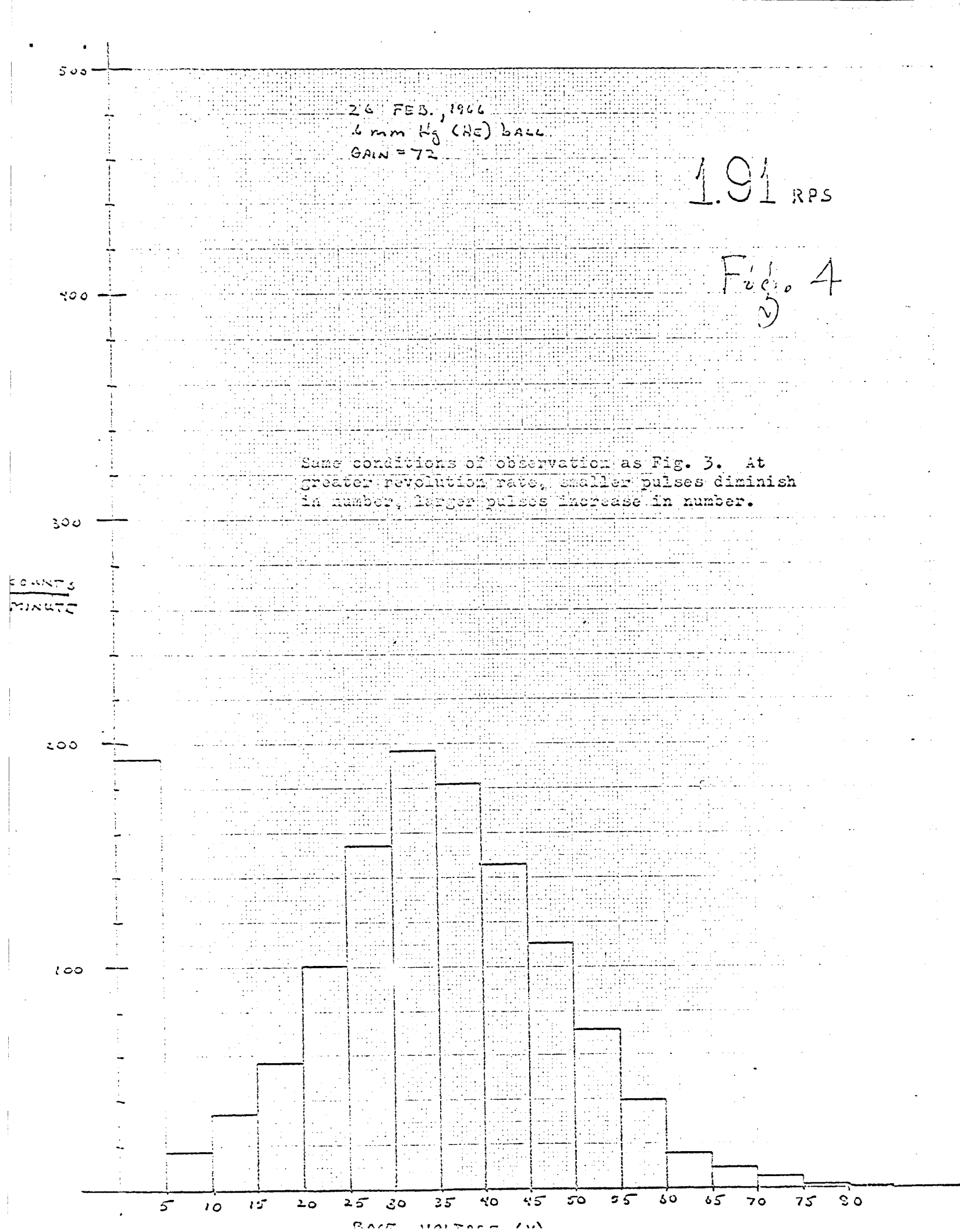
26 FEB., 1966
.6 mm Hg (He) BALL
GAIN = 72
1.91 RPS
Fig. 4
(2)
Same conditions of observation as Fig. 3. At greater revolution rate, smaller pulses diminish in number, larger pulses increase in number.
COUNTS / MINUTE
500
400
300
200
100
5
10
15
20
25
30
35
40
45
50
55
60
65
70
75
80
BASE VOLTAGE (V)

26 FEB., 1966
.6 mm Hg (HE) BALL
GAIN = 72

2.74 RPS

Fig. 5

Same conditions of observation as in Figs. 3 and 4. Trends of previous curves continue. Total number of pulses of all heights increases with angular velocity of the ball.

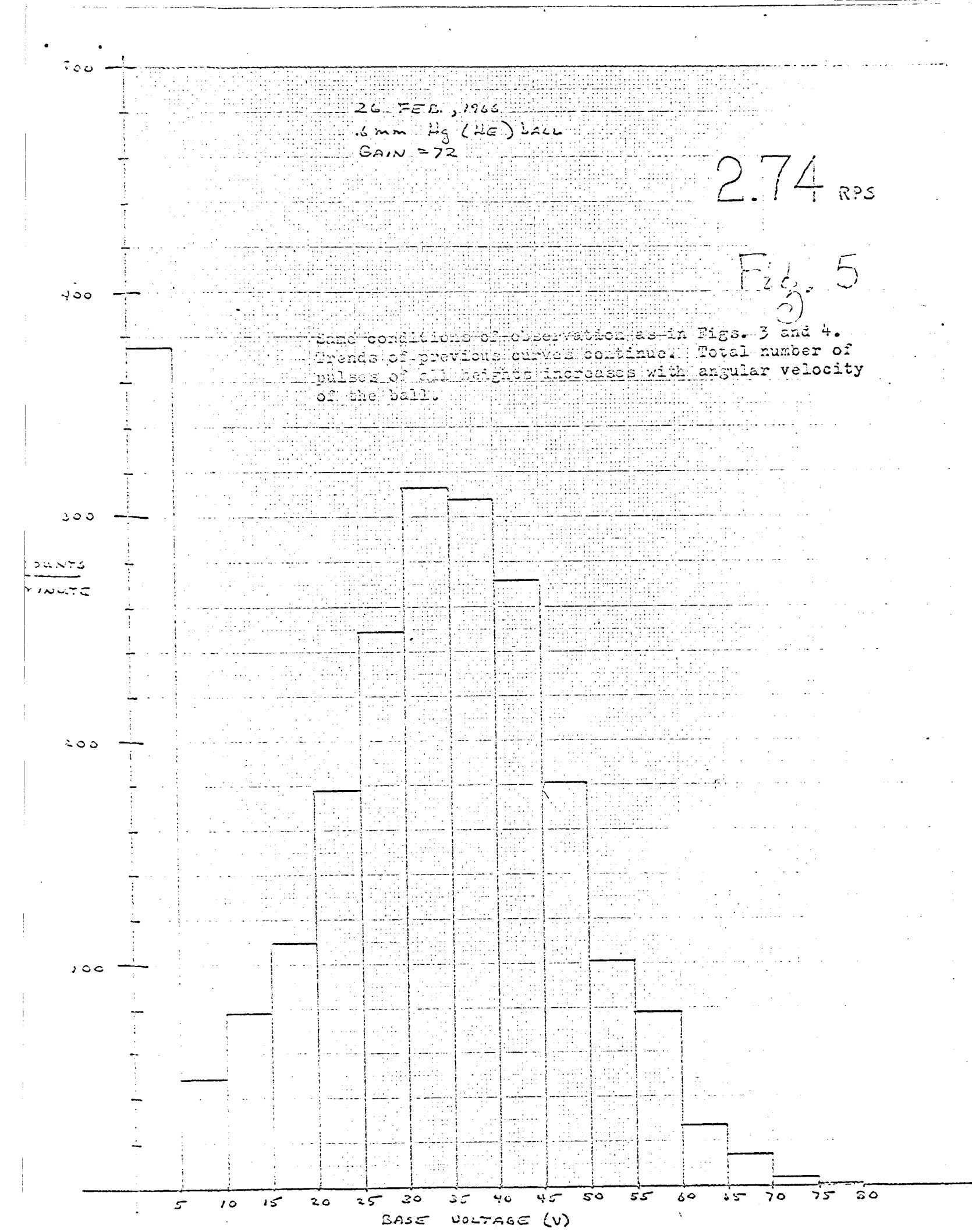

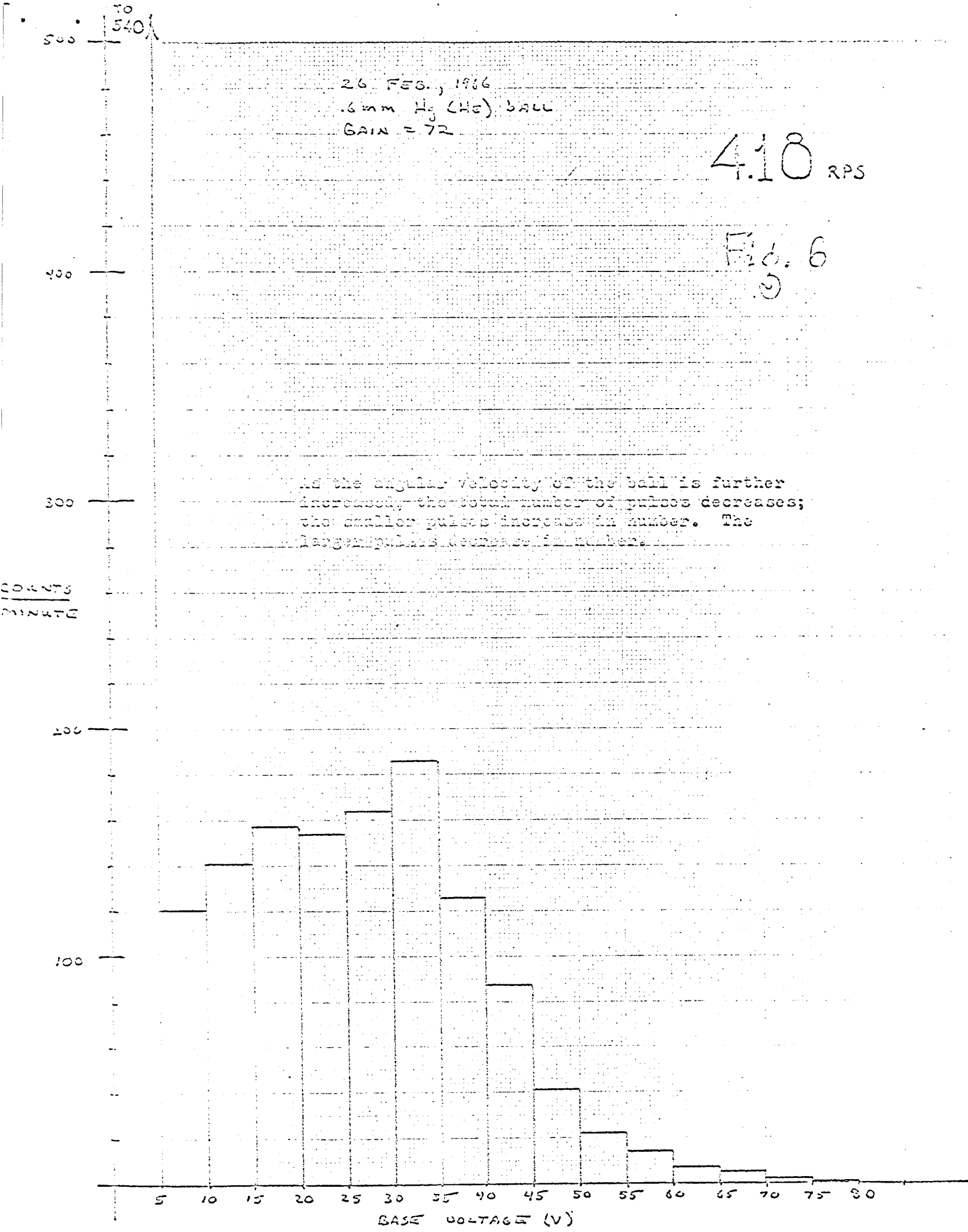
TO 540
500
400
300
200
100
26 FEB., 1986
.6 mm Hg (He) BALL
GAIN = 72
4.18 RPS
Fig. 6
3
As the angular velocity of the ball is further increased, the total number of pulses decreases; the smaller pulses increase in number. The larger pulses decrease in number.
COUNTS PER MINUTE
5 10 15 20 25 30 35 40 45 50 55 60 65 70 75 80
BASE VOLTAGE (V)

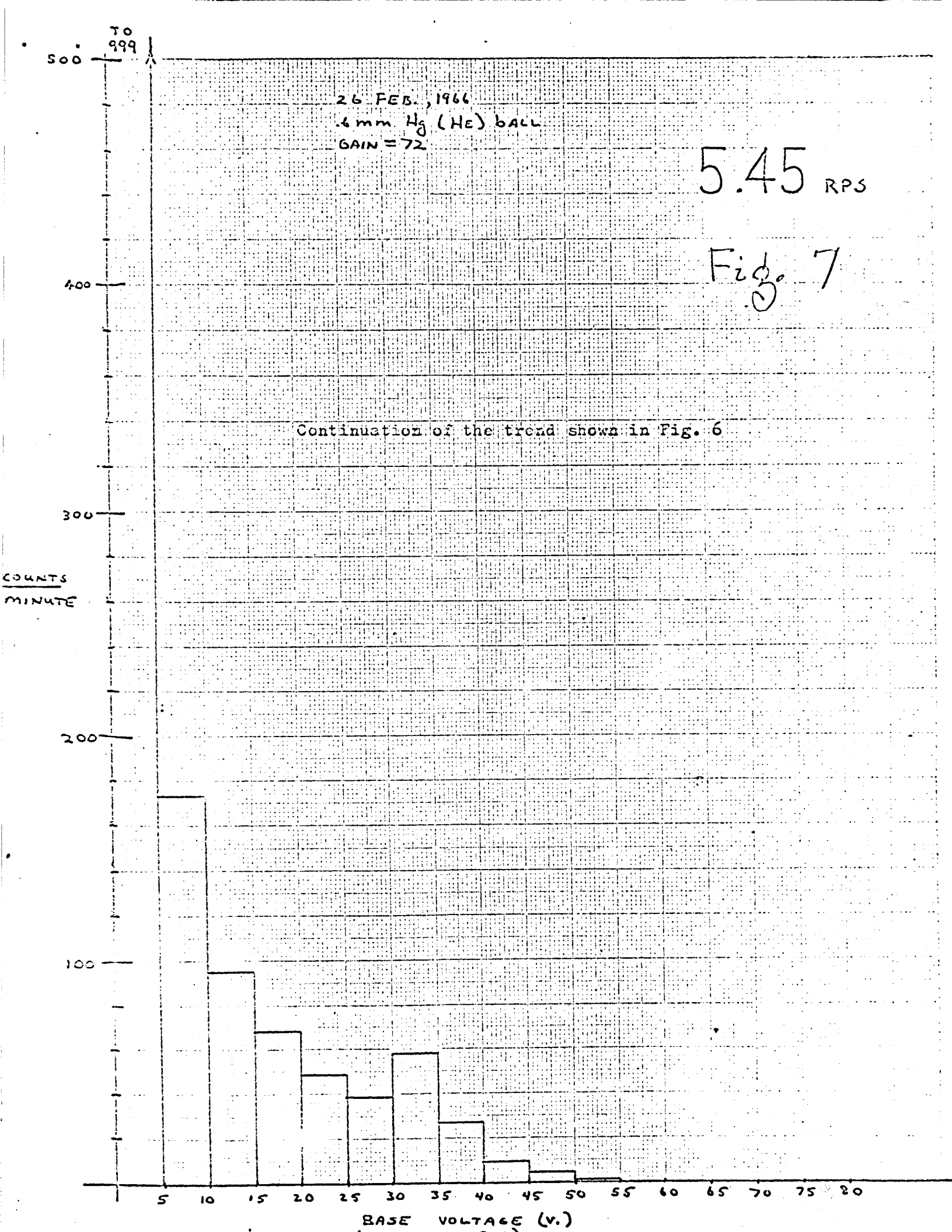
TO 999
500
400
300
200
100
COUNTS / MINUTE
26 FEB., 1966
.6 mm Hg (He) BALL
GAIN = 72
5.45 RPS
Fig. 7
Continuation of the trend shown in Fig. 6
5 10 15 20 25 30 35 40 45 50 55 60 65 70 75 80
BASE VOLTAGE (V.)

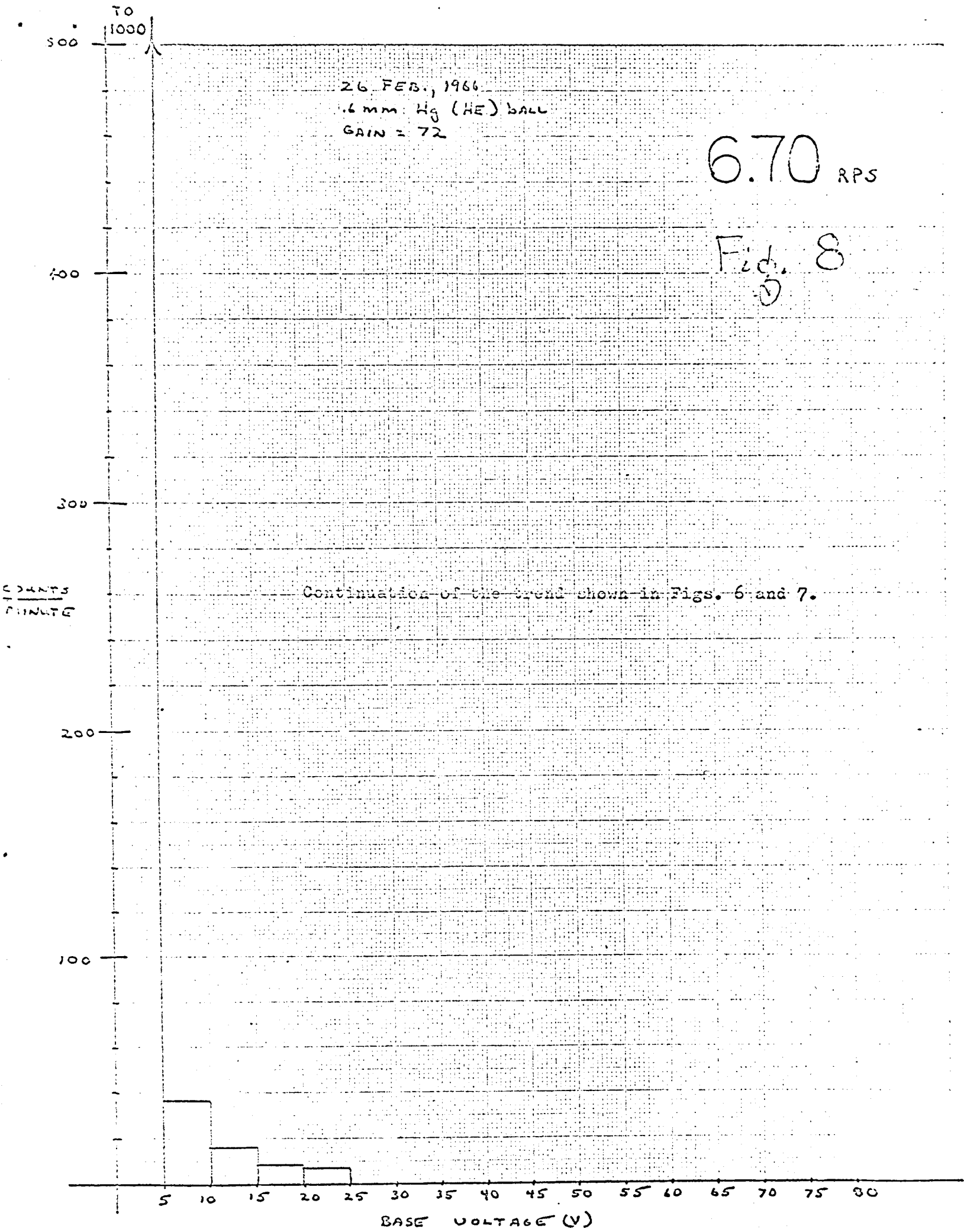
TO 1000
500
400
300
200
100
COUNTS / MINUTE
26 FEB., 1966
.6 mm Hg (HE) BALL
GAIN = 72
6.70 RPS
Fig. 8
Continuation of the trend shown in Figs. 6 and 7.
5 10 15 20 25 30 35 40 45 50 55 60 65 70 75 80
BASE VOLTAGE (V)

National Aeronautics and Space Administration NsG-692

Tracks of Heavy Ions in Emulsion, Physics Department,

Robert Katz, Principal Investigator

Status Report for the period March 1, 1966 to August 31, 1966

1) Measurements of the tracks of ions in emulsion by newly developed photographic techniques continue.
2) An additional stack of G-5 emulsion was exposed at balloon altitudes over Hudson's bay, courtesy Professor Peter Meyer, University of Chicago.
3) A seminar was presented at the Donner Laboratory on 10 May, and a paper was read at the III International Congress for Radiation Research, Cortina, Italy, 27 June, on the theory of Relative Biological Effectiveness for Heavy Ion Bombardment of Dry Enzymes and Viruses. A paper enlarging on this material has been submitted to Radiation Research.
4) A note entitled Simulated Radioactivity has been accepted by the American Journal of Physics.
5) A note entitled Magnetically Geared Microscope Stages has been accepted by the Review of Scientific Instruments.
6) Degree requirements have been completed by

J.J. Butts, Ph. D. , E.J. Kobetich, M. S.

Harvey Goldberg, M.S.

Reprints of all publications will be submitted when these become available.

Robert Katz

Robert Katz, Principal Investigator

National Aeronautics and Space Administration NsG-692
Department of Electrical Engineering
Principal Investigator - Dr. Charles A. Halijak

During the period from March 1, 1966 to August 31, 1966, this work was completed with the assistance of Burns E. Hegler, of the Electrical Engineering Faculty.

Initially, a considerable amount of time was devoted in determining the limits of the system and the theoretical effect of different order Butterworth filters upon these limits. The placement of the carrier frequency with respect to these limits was firmed up.

Much of the latter part of this period was devoted to the writing of a report of the findings. This report was published in our department as Technical Report No. 5, entitled "Ideal Single Sideband Modulation and Demodulation".

The report concluded that the model while was developed previously was feasible and that much more work remains to be done in this field. A copy of the report is attached.

KANSAS STATE UNIVERSITY
MANHATTAN, KANSAS

Technical Report EE-TR-5

IDEAL SINGLE SIDEBAND MODULATION AND DEMODULATION

BY

Charles A. Halijak

Burns E. Hegler

Department of Electrical Engineering

AUGUST, 1966

This work was partially
supported by NASA grant
NsG-692.

INTRODUCTION

We shall consider single sideband (SSB) modulation as a consequence of double sideband suppressed carrier (DSB) modulation. An outline of the DSB Laplace Transform formalism [1] will be presented and this is followed by a simple SSB theory. To be specific and to avoid excessive context, attention will be focussed on a case of upper sideband (USB) modulation.

There exists but one text [2] on SSB modulation. One can become acquainted with extensive past work by referring to this text and to References (3), (4), (5).

The simple flaw in this past work is due to unreasoning independence from DSB modulation theory. The latter theory is a necessary prerequisite to SSB modulation theory and liberates SSB modulation from unnecessary abstractions such as the analytic signal and Hilbert transforms [11].

DSB MODULATION FORMALISM

The ordinary Laplace Transform domain involves only addition and convolution operations. DSB modulation requires a real time multiplication operation. However, multiplication is a bilinear operation and this excessive generality is not suited to description of modulation systems. Linear operators can be obtained by restricted multiplication--only two functions of time, cos Ωt sin Ωt, will be multipliers; Ω is the carrier angular frequency.

Conventional Laplace Transform notation is unwieldy in this enlarged domain. It will be more efficacious to employ the R. V. Churchill notation

$$(1) \qquad \int_0^\infty e^{-st} f(t)\, dt = \bar{f}(s).$$

Compactness of notation is achieved because parentheses for variables can be dropped without ambiguity; i.e. $f(t) = f$ and $\bar{f}(s) = \bar{f}$. Moreover, notation economy is attained by reserving upper case letters for linear operators introduced by restricted multiplications.

Restricted multiplications in the Laplace Transform domain induce the following formulas and linear operators:

$$(2) \qquad \mathcal{L}[f(t)\cos \Omega t] = \frac{1}{2\pi j}\oint_R \bar{f}(\lambda)\frac{s-\lambda}{(s-\lambda)^2+\Omega^2}\, d\lambda \equiv C\bar{f} \quad ;$$

$$(3) \qquad \mathcal{L}[f(t)\sin \Omega t] = \frac{1}{2\pi j}\oint_R \bar{f}(\lambda)\frac{\Omega}{(s-\lambda)^2+\Omega^2}\, d\lambda \equiv S\bar{f} \quad .$$

The region R contains all poles of $\bar{f}(\lambda)$. Execution of these complex convolutions yields

$$(4) \qquad C\bar{f} = \text{Re}\ \bar{f}(s+j\Omega)$$

$$(5) \qquad S\bar{f} = \text{Im}\ \bar{f}(s-j\Omega).$$

These are called direct and quadrature Laplace transforms of f(t) respectively.

Besides distributivity of a linear operator over addition of signals, formulas for linear operations on transfer functions are possible; they are

$$(6a) \qquad \begin{aligned} C(\bar{g}C\bar{f}) + S(\bar{g}S\bar{f}) &= \bar{f}C\bar{g} \\ S(\bar{g}C\bar{f}) - C(\bar{g}S\bar{f}) &= \bar{f}S\bar{g}. \end{aligned}$$

These formulas mean that, "If $\overline{g}$ is a transfer function then $C\overline{g}$ and $S\overline{g}$ exist as transfer functions." Linear operations on convolutions, $\overline{f}\overline{g}$, are

$$(7a) \qquad \begin{aligned} C(\overline{f}\,\overline{g}) &= (C\overline{f})(C\overline{g}) - (S\overline{f})(S\overline{g}) \\ S(\overline{f}\,\overline{g}) &= (S\overline{f})(C\overline{g}) + (C\overline{f})(S\overline{g}) \quad . \end{aligned}$$

If $E \equiv \begin{pmatrix} C & S \\ -S & C \end{pmatrix}$, then matrix[6],[7] counterparts of these two sets of equations are

$$(6b) \qquad E^{-1}(\overline{g}E\overline{f}) = \overline{f}E^{-1}\overline{g} \ ,$$

$$(7b) \qquad E(\overline{f}\,\overline{g}) = (E\overline{f})(E\overline{g})$$

respectively and are convenient mnemonics.

Equation (7b) produces a result which will be useful in a later section. If one observes that $E1 = E^{o}$, the identity matrix, then

$$(8) \qquad E(1/\overline{f}) = (E\overline{f})^{-1} \ .$$

The main result of this section is that DSB signals and DSB transfer functions can be manipulated in the Laplace Transform domain enlarged by adjoinment of restricted multiplication[1].

IDEAL USB MODULATION AND DEMODULATION

The diagram in Fig. 1 is an ideal modulator and demodulator if $\overline{\mu}+\overline{\nu} = 1$. Note that the special transfer matrix E and its inverse, E^{-1}, are in cascade to form the identity matrix, E^{o}. One can readily replace these with direct connections and obtain the output, $(\overline{\mu}+\overline{\nu})\overline{f}$.

The $\overline{\mu}+\overline{\nu} = 1$ condition is not enough to ensure existence of pure USB terms on Channels 1 and 2! Only under special conditions will pure USB terms exist on these channels.

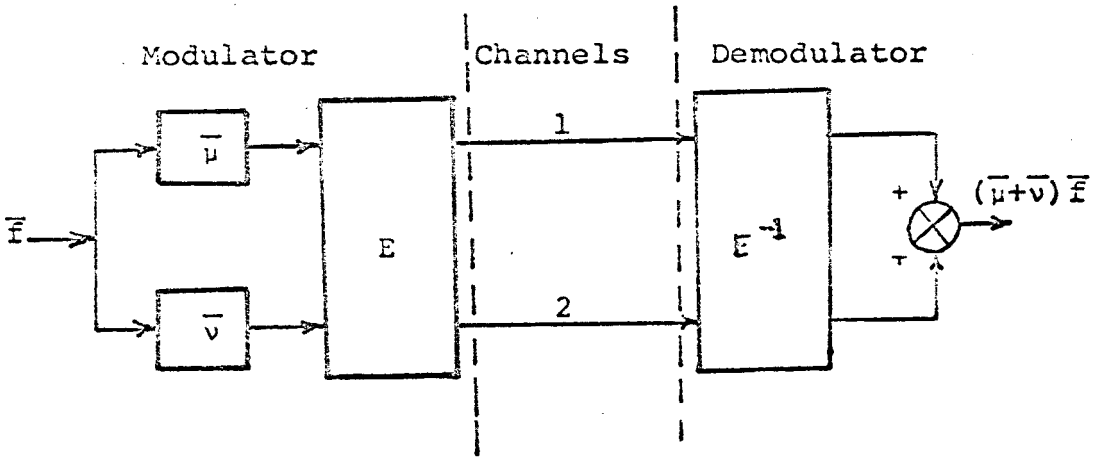

Fig. 1. An ideal modulator and demodulator

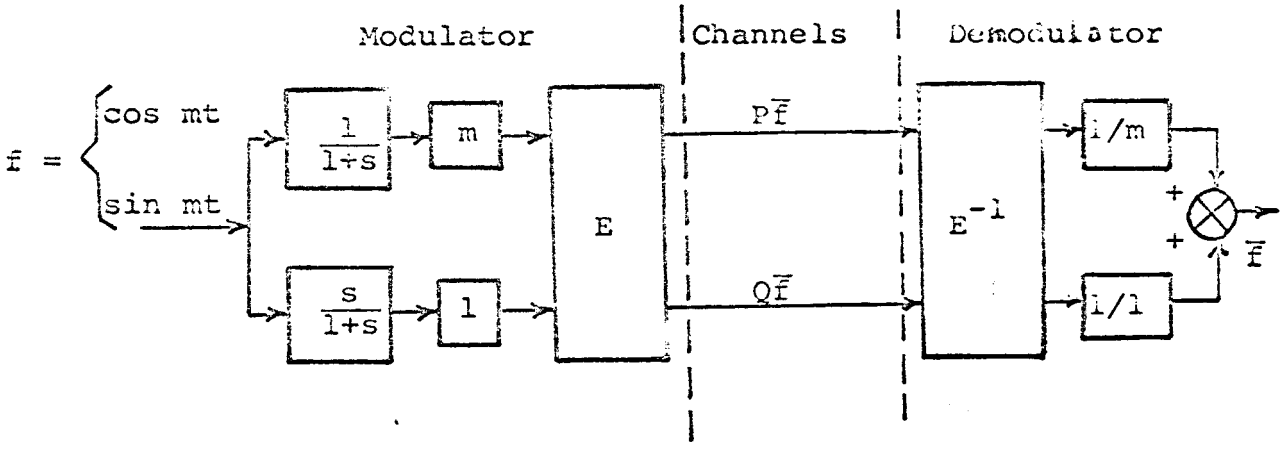

Fig. 2. An ideal USB modulator and demodulator with channel signals $P\bar{f}$ and $Q\bar{f}$

Consider the diagram of Fig. 2. Here, the input signal has been restricted to cos mt; E has been premultiplied by the matrix $\begin{pmatrix} m & 0 \\ 0 & 1 \end{pmatrix}$; and E^{-1} has been postmultiplied by $\begin{pmatrix} m & 0 \\ 0 & 1 \end{pmatrix}^{-1}$. Channel signals are identified as $P\bar{f}$ and $Q\bar{f}$ respectively. The following two theorems can be stated.

Theorem 1. If $\bar{f} = s/(s^2+m^2)$, $\bar{\mu} = 1/(1+s)$, $\bar{\nu} = s/(1+s)$ in Fig. 2 and

$$(9) \qquad \begin{aligned} P\bar{f} &\equiv C(m\bar{\mu}\bar{f}) + S(\bar{\nu}\bar{f}) \\ Q\bar{f} &\equiv -S(m\bar{\mu}\bar{f}) + C(\bar{\nu}\bar{f}) \end{aligned} .$$

then the steady-state forms of $P\bar{f}$ and $Q\bar{f}$ are USB signals.

Proof. Straightforward calculations employing the DSB formalism yield

$$(10) \qquad 2P\bar{f} = \frac{\Omega^2+s+s^2}{\Omega^2+(1+s)^2} \cdot \frac{\Omega+m}{s^2+(\Omega+m)^2} - \frac{\Omega}{\Omega^2+(1+s)^2} \cdot \frac{s}{s^2+(\Omega+m)^2}$$

$$(11) \qquad 2Q\bar{f} = \frac{\Omega^2+s+s^2}{\Omega^2+(1+s)^2} \cdot \frac{s}{s^2+(\Omega+m)^2} + \frac{\Omega}{\Omega^2+(1+s)^2} \cdot \frac{\Omega+m}{s^2+(\Omega+m)^2} .$$

Sine and cosine terms have angular frequencies $(\Omega+m)$ and no $(\Omega-m)$ angular frequencies are present.

It is apparent that the time constant of the filter (normalized to 1) will determine damping of the transient term and will effect the amplitude and phase angle of steady state terms. These latter effects do not alter ideality of our SSB modulator and demodulator.

Theorem 2. If $\bar{f} = m/(s^2+m^2)$, $\bar{\mu} = 1/(1+s)$, $\bar{\nu} = s/(1+s)$ in Fig. 2 and

$$\begin{aligned} P\bar{f} &\equiv C(m\bar{\mu}\bar{f}) + S(\bar{\nu}\bar{f}) \\ Q\bar{f} &\equiv -S(m\bar{\mu}\bar{f}) + C(\bar{\nu}\bar{f}) \end{aligned}$$

then the steady-state forms of $P\overline{f}$ and $Q\overline{f}$ are upper sideband (USB) signals.

Proof. Straightforward calculation yields

$$(12) \qquad 2P\overline{f} = \frac{m(1+s)}{\Omega^2+(1+s)^2} \cdot \frac{\Omega+m}{s^2+(\Omega+m)^2} + \frac{m\Omega}{\Omega^2+(1+s)^2} \cdot \frac{s}{s^2+(\Omega+m)^2}$$

$$(13) \qquad 2Q\overline{f} = \frac{-m\Omega}{\Omega^2+(1+s)^2} \cdot \frac{\Omega+m}{s^2+(\Omega+m)^2} + \frac{m(1+s)}{\Omega^2+(1+s)^2} \cdot \frac{s}{s^2+(\Omega+m)^2} .$$

There will be no angular frequencies $(\Omega-m)$ present and the theorem is established.

These two theorems establish invariance of these USB channel signals to input signal phase shifts.

Since the ideal modulator/demodulator requires both m and 1/m, it is necessary that m be neither very small nor very large. This observation results in a simple corollary.

Corollary. Input signal data angular frequencies are necessarily restricted to a passband determined by some small number $\underline{m}$ such that $0<\underline{m}/\Omega<1$. This passband is the angular frequency interval $(\underline{m}/\Omega, \Omega/\underline{m})$.

A procedure for determining $\underline{m}$ will be presented in a subsequent section.

DEVIATION OF CHANNEL SIGNALS FROM IDEAL SSB

If m is fixed in the modulator/demodulator and the input signal is cos nt and n differs from m, then it is impractical to change constants m and 1/m and other means for reducing unwanted lower sideband (LSB) contaminants need to be proposed.

We shall first remark that LSB contaminants exist in the P- and Q- channels. Ensuing calculations require trigonometric

formula types in the following lemma.

Lemma: If A, B are positive real numbers and $T_1 = A \sin\theta\cos\Psi + B \cos\theta\sin\Psi$, then $2T_1 = (A-B)\sin(\theta-\Psi)+(A+B)\sin(\theta+\Psi)$. If A and B are positive real numbers and $T_2 = A \cos\theta\cos\Psi - B \sin\theta\sin\Psi$, then $2T_2 = (A-B)\cos(\theta-\Psi)+(A+B)\cos(\theta+\Psi)$. Note that sum amplitudes are associated with sum angles and that difference amplitudes are associated with difference angles.

Theorem 3. If the input signal is cos nt or sin nt and constants m and 1/m are fixed in the ideal USB modulator of Fig. 2 then the ratio of undesired LSB signal amplitude is $|(n-m)/(n+m)|$.

Since n is restricted not to approach zero, one can obtain the proper inequality

$$\left|\frac{n-m}{n+m}\right| < 1 \quad . \tag{14}$$

This result contrasts with Nyquist's Vestigial-Sideband (VSB) modulation[8] wherein a similar ratio is identical to one. However, a sharp cut-off filter is used to lessen the unity value of this ratio. Similar filters can be placed in P- and Q-channels of our ideal USB modulator for further reduction of LSB/USB. Study of such modified modulator will be pursued in the following sections.

USB MODULATOR WITH CHANNEL FILTERS

A modified ideal USB modulator which transmits more than one angular frequency is obtained by addition of high-pass filters, $\bar{h}$, to P- and Q-channels. These new channels signals are $\bar{h}P\bar{f}$ and $\bar{h}Q\bar{f}$. The result is shown in Fig. 3.

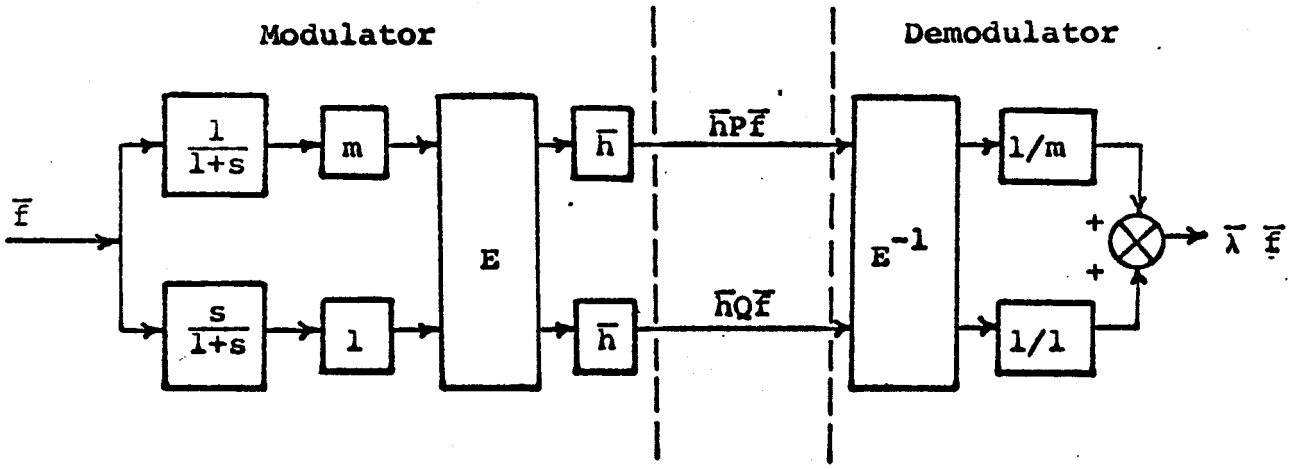

Fig. 3. Modified USB modulator and demodulator.

Two basic problems are placement of the filter cut-off frequency relative to the carrier frequency and calculation of the least upper bound of the previously defined $\underline{m}$ dependent on the fact that practical filters have finite slopes near cut-off frequencies.

In order to present concepts without difficult calculations, filters, $\bar{h}$, will belong to the class of Butterworth filters. Ultimately, sharper cut-off filters such as Chebyshev or mechanical resonator filters should be employed in actual physical systems.

A Butterworth high pass filter of order k and cut-off frequency, ω_o, possesses a spectrum of the form $1/\sqrt{1+(\omega_o/\omega)^{2k}}$. The required ratio follows directly from the trigonometric lemma and $\bar{h}P\bar{f}$ and $\bar{h}Q\bar{f}$ formulas:

$$(15) \qquad \frac{LSB}{USB} = \left|\frac{n-m}{n+m}\right| \frac{\sqrt{1+\left[\frac{\omega_o}{\Omega+n}\right]^{2k}}}{\sqrt{1+\left[\frac{\omega_o}{\Omega-n}\right]^{2k}}} < \left|\frac{n-m}{n+m}\right|$$

A direct attack on this ratio requires that $\frac{\omega_o}{\Omega+n} < \frac{\omega_o}{\Omega-n}$; but since $\omega_o > 0$ and $0 < n < \Omega$, this inequality is tautologous and another approach is required to resolve our two basic filter problems.

The spectrum of any Butterworth high-pass filter has the shape of a sigmoid. This spectrum can be approximated by three line segments: one line segment is of zero slope and zero amplitude; the next line segment has finite positive slope and extends from zero to unity amplitudes; and the third line is of zero slope

and unity amplitude. Intersections of the second line segments with the first and third line segments define corner frequencies ω_{CL} and ω_{CU} for the lower and upper corner frequencies respectively.

The second line segment will be placed at the inflection point of the Butterworth spectrum and the second line segment's slope will be the slope of the Butterworth spectrum at the inflection point.

A straightforward analysis of a Butterworth spectrum of order k yields information about the second line segment's placement and slope and also about corner frequencies:

(a) inflection point occurs at $\omega_o \left[\frac{k-1}{2k+1}\right]^{1/2k}$;

(b) the inflection point has amplitude

(16) $$\sqrt{(k-1)/3k} \leqslant 0.577350 \quad ;$$

(c) the lower corner frequency is given by

(17) $$\frac{\omega_{CL}}{\omega_o} = 2\left[\frac{k-1}{2k+1}\right]^{1+(1/2k)} < 1 \quad ;$$

(d) the positive difference of corner frequencies is

(18) $$\omega_{CU} - \omega_{CL} = \omega_o \left[\frac{3}{2k+1}\right]\left[\frac{3k}{k-1}\right]^{1/2}\left[\frac{k-1}{2k+1}\right]^{1/2k} .$$

It should be noted that the last formula is the multiplicative inverse of the slope at the inflection point.

In order to make LSB/USB nearly infimal, the carrier frequency should be placed on the first line segment to the left of ω_{CL} and m should be chosen large enough so that $\Omega+m$ is on the third line segment to the right of ω_{CU}. Since the slope

at the inflection point is the largest slope, one can then state that

(19) $$g.l.b.\Omega=\omega_{CL}$$

(20) $$l.u.b\ \underline{m}=\omega_{CU}-\omega_{CL}\ .$$

This polygonal approximation can be refined by adjoining more line segments; this will result in lower ω_{CL} and higher $\omega_{CU}-\omega_{CL}$. Thus does one verify these greatest lower bound (g.l.b.) and least upper bound (l.u.b) assertions.

Table 1 shows values of ω_{CL}/ω_o and $(\omega_{CU}-\omega_{CL})/\omega_o$ for different orders of Butterworth filters. It is evident that filter order should be 32 before desirable values close to one and zero are achieved.

Table 1. Values of ω_{CL}/ω_o and $(\omega_{CU}-\omega_{CL})/\omega_o$ for k-th order Butterworth filters.

k	ω_{CL}/ω_o	$(\omega_{CU}-\omega_{CL})/\omega_o$
2	0.26749	0.98284
4	0.58112	0.58112
8	0.77910	0.30913
16	0.88696	0.15866
32	0.94287	0.08028
64	0.97129	0.04037
.	.	.
.	.	.
.	.	.
∞	1.0	0

The contaminant ratio, d, can be readily calculated. However, the shape of the graph is more apparent when low order Butterworth filters are employed. An exemplary calculation for k=2 results in the graph of Fig. 4. Note that $\Omega>n\geq m$ is more

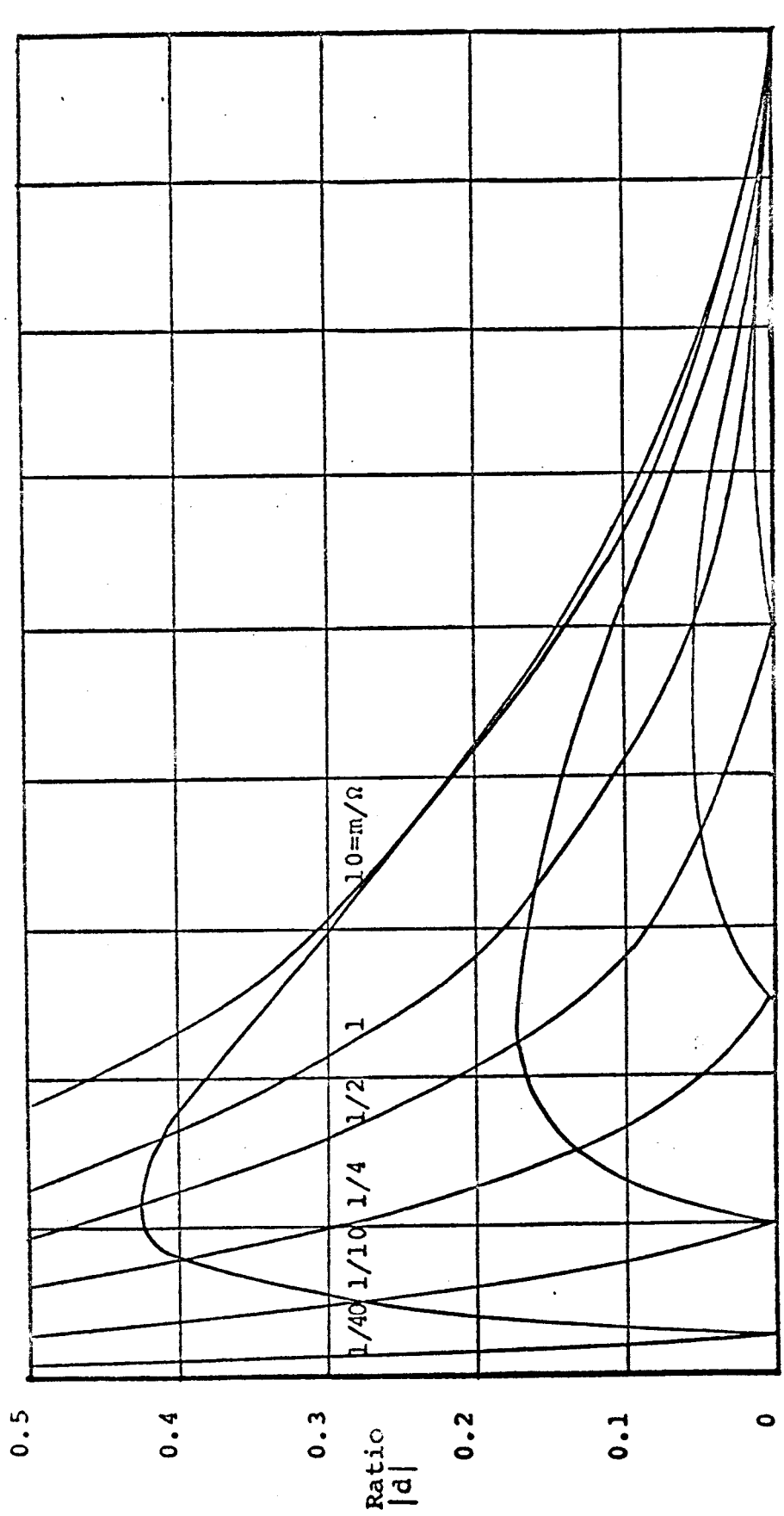

Fig. 4 Contaminant ratio for a second order Butterworth filter.

desirable than n<m. This observation suggests that the constant m should be the lower (necessarily greater than l.u.b m) angular frequency of input data band-pass angular frequencies.

DIRECT AND QUADRATURE NATURE OF CHANNEL SIGNALS

Calculations of $P\bar{f}$ and $Q\bar{f}$ for $\bar{f} = s/(s^2 + n^2)$ in the ideal USB modulator of Fig. 2 yield

$$(21)\quad \begin{pmatrix} 2P\bar{f} \\ 2Q\bar{f} \end{pmatrix} = \begin{pmatrix} S\bar{\nu} & C\bar{\nu} \\ C\bar{\nu} & -S\bar{\nu} \end{pmatrix} \left[\frac{1-(m/n)}{s^2+(\Omega-n)^2} \begin{pmatrix} s \\ \Omega-n \end{pmatrix} + \frac{1+(m/n)}{s^2+(\Omega+n)^2} \begin{pmatrix} s \\ \Omega+n \end{pmatrix} \right] .$$

Since the matrix in the above equation is almost its own inverse, i. e.

$$(22)\quad \begin{pmatrix} S\bar{\nu} & C\bar{\nu} \\ C\bar{\nu} & -S\bar{\nu} \end{pmatrix} \begin{pmatrix} S\bar{\nu} & C\bar{\nu} \\ C\bar{\nu} & -S\bar{\nu} \end{pmatrix} = \begin{pmatrix} (C\bar{\nu})^2 + (S\bar{\nu})^2 & 0 \\ 0 & (C\bar{\nu})^2 + (S\bar{\nu})^2 \end{pmatrix}$$

one can conclude that insertion of the channel transfer function matrix

$$(23)\quad \frac{1}{(C\bar{\nu})^2+(S\bar{\nu})^2} \begin{pmatrix} S\bar{\nu} & C\bar{\nu} \\ C\bar{\nu} & -S\bar{\nu} \end{pmatrix} = \begin{pmatrix} -S(1/\bar{\nu}) & C(1/\bar{\nu}) \\ C(1/\bar{\nu}) & S(1/\bar{\nu}) \end{pmatrix}$$

will result in cosinusoids in the P-channel and sinusoids in the Q-channel. Equation (23) is a rearranged form of Equation (8). It is apparent that there is no further need for cross-couplings of P- and Q-channels. The contaminant ratio will be invariant.

Signals $P\bar{f}$ and $Q\bar{f}$ are somewhat analogous to $C\bar{f}$ and $S\bar{f}$ respectively although the full apparatus of this analogy is not at all required for ideal SSB modulation.

MODIFIED USB MODULATOR-DEMODULATOR'S TRANSFER FUNCTION

If the ideal USB device of Fig. 3 is considered and appli-

cation made of formulas for existence of transfer functions $C\bar{g}$ and $S\bar{g}$, then this device's transfer function, $\bar{\lambda}$, is found to be

$$(24) \qquad \bar{\lambda} = (\bar{\mu}+\bar{\nu})C\bar{h} + [m\bar{\mu}-(\bar{\nu}/m)]\ S\bar{h} \quad .$$

Since $\bar{\mu} + \bar{\nu} = 1$, one obtains

$$(25) \qquad \bar{\lambda} = C\bar{h} + [m\bar{\mu} - (\bar{\nu}/m)]\ S\bar{h} \quad .$$

This transfer function is rather tedious to compute for arbitrary order Butterworth filters and its study is deferred to some future time.

LSB MODULATION

An USB modulator has been chosen to exemplify SSB modulators in previous sections. There exist corresponding LSB modulators! For instance, if E is replaced by E^{-1} and high-pass channel filters are replaced by low-pass filters, then a LSB modulator results. Of course, there exists a dual of our lemma.

Perhaps the most common communication channel is the telephone transmission line. The lowest quality telephone line is an RC transmission line while a high quality telephone line is the Pupin line--an RC line with series loading coils. In any event, the telephone transmission line behaves like a low-pass filter and LSB modulation is the pertinent modulation scheme for the telephone line. These facts have been exploited by Rixon Electronics, Inc. of Silver Spring, Maryland for digital data transmission.

It is appropriate to question relevance of Butterworth filter simulation of telephone lines! The Butterworth filter

can be considered a second order approximation of the loss-less LC line and is a degraded form of the LC line because it does not possess the linear phase angle property. Since losses can be regained by repeaters, one can simulate telephone lines with symmetric, loss-less two-ports which are left and right terminated in equal resistors. Such Butterworth filter synthesis has been accomplished by Bennett[9] in 1932.

However, the next theorem, due to Larry B. Hofman, is required for completeness.

Theorem 4. Only Butterworth filters of order k_n where $k_o = 3$, $k_n = k_{n-1} + 4$, $n = 1, 2, 3, \ldots$, realizable as symmetric two-ports, have characteristic impedances whose spectra are monotonic approximations to given constants (resistances) in the pass band. (These are the preferable constant-resistance networks.)

An immediate consequence of Hofman's theorem is that Butterworth filters or order 31, 35, 39, 43,...are admissible channel filters. This follows from our observation that a filter of order 32 begins to produce acceptable values for ω_{CL}/ω_o and $(\omega_{CU}-\omega_{CL})/\omega_o$.

CONCLUDING REMARKS

An example of an ideal upper sideband modulator has been presented and consequences were developed therefrom. Much work remains to be done in order to uncover facts hidden by tedious calculations of the transfer function $\bar{\lambda}$.

It is noteworthy that double phasor concepts from DSB modulation such as envelope spectrum, envelope phase angle

and carrier phase angle [10] are absent in the given SSB model. Direct and quadrature Laplace transforms and single phasors characterize this SSB modulator completely.

Single channel SSB modulators are often employed for equipment economy. These modulators are necessarily degraded forms of ideal two channel modulators and their performance specifications are hopelessly incomplete unless an ideal modulator is used as a performance reference.

REFERENCES

1. C. A. Halijak, Linear Operator Analysis of Carrier-Frequency Servomechanisms, Dissertation, Electrical Engineering Department, University of Wisconsin, Madison, Wisconsin, June, 1956, pp 56-66.

2. E. W. Pappenfus, W. B. Bruene and E. O. Schoenike, Single Sideband Principles and Circuits, McGraw-Hill Co., New York, 1964.

3. I. J. Kaar, Single-Sideband Issue, Proceedings IRE, Vol. 44, No. 12, pp 1666-1873, December 1956.

4. R. F. Filipowsky and L. C. Bickford, Single Sideband Modulation, Space Communications: Theory and Applications. Volume 1: Modulation and Channels, NASA SP-7022(01), Section 1.223, pp 61-66, June 1965.

5. Fundamentals of Single Side Band, NAVSHIPS 93271, Bureau of Ships, Navy Department, Washington, D. C., September 1958, Chapter I, pp 1-17.

6. S. Perlis, Theory of Matrices, Addison-Wesley Press, Inc., Cambridge, Mass., 1952.

7. H. H. Hosenthien, Analysis of Carrier Systems by Modulation Equivalent Transfer Matrices, Report 1R10, Army Ballistic Missile Agency, Redstone Arsenal, Huntsville, Alabama, March 1956, pp 1-57.

8. H. S. Black, Modulation Theory, D. Van Nostrand Company, Inc., Princeton, New Jersey, 1953, pp 22-24.

9. W. R. Bennett, Transmission Network, U. S. Patent No. 1,849,656, March 1932, pp 1-7.

10. C. A. Halijak and T. J. Higgins, AC Control System Analysis by Use of Trigonometric Forms, ISA Transactions, Vol. 4, No. 4, October, 1965, pp. 378-383.

11. M. S. Corrington, Properties and Applications of Hilbert Transforms, Radio Corporation of America, EM8333, June 1962, pp 9-39.

DETERMINATION OF OPTIMUM NOZZLE CONTOURS FOR THE EXPANSION OF DISSOCIATED GAS BY METHODS OF THE VARIATIONAL CALCULUS

Dr. James M. Bowyer, Jr., Mechanical Engineering Department

NASA NsG-692

Fourth Semi-annual Report

During the past half year, the thesis of Mr. Bong L. Koh entitled "Supersonic Base Drag in the Presence of Base Burning" has been successfully defended. Since part of the support for this research was furnished by NsG-692 funds, a copy of this thesis was forwarded to Dr. John T. Holloway of the Office of Grants and Research Contracts NASA on August 4, 1966.

The abstract submitted to the XVIIth International Aeronautical Congress earlier this year has resulted in an invitation to present the results of the investigation reported by Richard R. Berns in his thesis as extended by the projects' principal investigator. A copy of the paper to be presented in Madrid on October 13, 1966 is enclosed. Additional copies of this paper will be made available at the request of the project monitor.

Mr. Norbert W. Deneke has joined the principal investigator in the studies funded by this portion of Grant NsG-692. His efforts up to this time have been directed towrad gaining an understanding of tasks previously completed under this project. He is currently beginning an intensive study of the kinetics of hydrogen-oxygen chemical reaction.

"Determination of Optimum Nozzle Contours for the Expansion of Dissociated Gases by Methods of the Variational Calculus"

Richard R. Berns* and James M. Bowyer, Jr. **
Kansas State University, Manhattan, Kansas

Abstract

Optimum nozzle contours have been obtained for the expansion of a Lighthill idealized dissociating gas in one-dimensional flow. Both uncatalyzed and catalyzed reactions have been considered. A characteristic density and reaction rate were selected for this gas so as best to represent the behavior of hydrogen over the temperature range considered in the investigation. The nozzle contours are optimum in the sense that, for given initial conditions and given reaction rate, propellant specific impulse is a maximum for a nozzle of given length operating under balanced pressure conditions at the nozzle exit, i.e., with nozzle exit static pressure equal to the ambient atmospheric pressure. Because the variational problem is of the Mayer type, one optimum nozzle contour can be considered to be the solution for one set of initial conditions and one reaction rate but for many different nozzle lengths and corresponding exit pressures. This is not entirely advantageous, because the nozzle is optimum in the sense of providing maximum specific impulse in a given length nozzle only when it is stipulated that the nozzle exit pressure is equal to the ambient atmospheric pressure.

Using the same Lighthill idealized dissociating gas model for hydrogen as was specified for the optimum nozzle calculations, further comparison calculations have been made for nozzles whose supersonic sections are

* Presently Research Specialist, Aerospace Group, Space Division, The Boeing Company, P. O. Box 3868, Seattle, Washington

** Professor, Department of Mechanical Engineering, Associate Fellow AIAA

This work has been supported by NASA Multi-Disciplinary Grant No. NsG-692.

hyperbolic and each of which has a length, exit area ratio, and ambient atmospheric pressure equal to that of the optimum nozzle with which it is compared.

A nuclear rocket utilizing a vortex-contained gas-phase reactor has been assumed. Thus, a stagnation temperature of 9000° R and a stagnation pressure of 600 psia were employed in the study. The length required for an optimum nozzle in the case of the expansion of uncatalyzed hydrogen to an ambient pressure representative of earth orbital and escape trajectories is prohibitive, e.g., 84 meters. However, in the case of the expansion of hydrogen in the presence of a potent catalyst, the required length for an optimum nozzle exhausting to the same ambient pressure is only 1.2 meters and is thus of practical interest.

The latest results of this investigation indicate that a gain of only a few tenths of one percent in balanced-pressure specific impulse can be realized by utilizing an optimum nozzle contour instead of the best hyperbolic contour of the same length.

On the other hand, if a potent catalyst for the hydrogen reassociation reaction at high temperature can be found, great reductions in required nozzle length (whether of optimum or hyperbolic contour) for a given specific impulse can be achieved. The resultant weight-reduction which could be realized in the nozzle of a rocket engine of the type investigated here would then be very significant.

Introduction

Only the briefest review of the investigation on which this report is based is possible here. For this reason, neither the definitions of symbols nor the list of references is complete. The choice of symbols is believed to be consistent with the literature cited and usual usage. The references

included are believed to be those most closely related to the investigation reported here.

The Medium

The behavior of any real gas at high temperature is complex, and a precise description of its behavior is correspondingly difficult to obtain and cumbersome to employ. By making several astute approximations, Lighthill[1] obtained an analytic description for an 'idealized' dissociating diatomic gas and showed that this model provided a reasonably accurate approximation to the real behavior of oxygen or nitrogen over a considerable range of temperature at moderate pressures. Lighthill's assumptions and corresponding analytic description are summarized in Fig. 1.

In the study presented here, the real behavior of hydrogen has been approximated by a suitably matched Lighthill-type model. The suitability of the model can be judged by the reader himself from a consideration of (1) the data, (2) the requirement that $(\bar{u} - \frac{D}{2m} \alpha)/(\frac{k}{m} \bar{T})$ equal 1.5, and (3) the present authors' choice of $\bar{\rho}_d$. This information is presented in Fig. 2.

Because the Lighthill-type model employed here is approximate, more significance should be attributed to the trends than to the numerical values of the various problem parameters in the results presented below.

The Flow

Bray's equations[2] for the one-dimensional, non-viscous, adiabatic flow of an 'idealized' dissociating diatomic gas have been employed in the investigation reported here and are shown in Fig. 3.

The first equation is derived from the continuity equation with the aid of the mass, momentum, and energy conservation equations and the equations describing the state and specific enthalpy of the gas.

The second equation is the reaction rate equation for the gas. The

first term on the right side of the equation presented here is really Bray's rate equation multiplied by the factor, $1 + \alpha$; this form is consistent with Clarke's reaction rate equation[3] and considers atoms to be fully as effective (rather than only one-half as effective) as molecules in the collisions which result in dissociation or reassociation. The second term on the right side of the reaction rate equation has been derived by R. R. Berns[4] and accounts for the increase in the reaction rate of an 'idealized' dissociating gas induced by a small mass fraction of a potent catalyst. Together with others, a paper by Girouard[5] provided a basis for Berns' derivation.

The third of Bray's equations specifies the area distribution in the nozzle; thus, A is the control variable used by Bray. Alternatively, the specific enthalpy, i, can be employed as a control variable; in fact, this is the only valid choice in that region of the nozzle where local speed is approximately equal to the local frozen speed of sound and $Q(i,\alpha)$, the coefficient of i' in the flow equation, is approximately zero. Note that the space rate-of-change of the mass fraction dissociated, α', is defined by the reaction rate equation; therefore, it cannot be employed as a control variable and does constitute a reasonable parameter for extremization. In this regard, a paper by Kelley is recommended.[6]

The Variational Problem

The variational problem which was initially posed was this:

> Given an 'idealized' dissociating diatomic gas at specified stagnation conditions, what nozzle contour should be provided to a nozzle of given length so as to obtain the highest possible specific impulse?

Given the gas, the catalyst if one is employed, and specified stagnation

conditions, the specific impulse is a function only of the conditions at the end of the nozzle as can be seen from Fig. 4. For given initial conditions and given ambient pressure, p_a, it is clear that I_{SP} will be a maximum at any given distance down the nozzle if I_{SP} has been maintained at its maximum possible value at every point along the length of the nozzle. The corresponding variational problem is called a Mayer problem [4,6].

To maximize specific impulse at any point along the nozzle, subject to the constraining flow and reaction rate equations, a Lagrange function of the form shown in Fig. 5 is employed. Since the functions, f and g, are differential functions, the associated multipliers λ and μ must be considered to be functions of ξ. The three Euler equations obtainable from the Lagrange function are also shown in Fig. 5.

On the surface, the two constraint equations and the three Euler equations appear to constitute a set of five first-order ordinary differential equations in the five unknowns, i, α, A, λ, and μ. But whenever the quantity to be extremized is a function only of the dependent variables, that quantity disappears identically from the Euler equations; thus, the Lagrange function could just as well have been chosen to be $F = \lambda f + \mu g$. Now it is clear that λ and μ are not independent and that only their ratio is significant. Also, whenever the function to be extremized is a function of the dependent variables only, a first integral exists. In the present problem, the first integral yields $\mu = 1/\Gamma$. Using this formula for μ, if the second and third of the Euler equations shown in Fig. 5 are solved for A' and i', respectively, and if the latter results are then substituted into the flow equation, a formula for λ in terms of i, α, and A can be obtained.

Because of the constraints imposed by the reaction and flow equations,

analysis by the usual method shows that only one natural end condition exists for the optimization of specific impulse or thrust:

> The static pressure of the gas as it leaves the exit plane of the nozzle must be equal to the ambient pressure.

The Boundary Value Problem

The boundary value problem resulting from the foregoing analysis is summarized in Fig. 6. The existence of a variety of options and intracacies associated with starting and continuing the actual numerical solution of this boundary value problem is hidden behind this summary. In order to obtain an initial condition for the flow in the nozzle, equilibrium flow must be assumed from stagnation conditions to some initial section; then these equilibrium conditions must be perturbed to allow initiation of the finite-rate chemically reacting flow [2,4]. When a finite reaction rate is employed upstream of the nozzle throat, determination of the mass flux density at the throat must be made (1) by trial-and-error, or (2) the results must be normalized after the uncorrected solution is obtained so as to make the dimensionless throat area equal to unity.

The required constants (three for uncatalyzed flow or five for catalyzed flow), the three initial conditions and corresponding three governing differential equations, and the algebraic equation defining the remaining Lagrange multiplier are presented in Fig. 6. Wherever Γ or λ has been subscripted with i, α, or A, the corresponding partial derivative is indicated.

The flow conditions resulting from the expansion of idealized dissociating hydrogen, in the absence or presence of a catalyst, through each of the comparison hyperbolic nozzles were determined by the methods described by Bray[2].

The Calculations

The stagnation conditions selected were $\bar{T}_o = 9000^o$ R and $\bar{p}_o = 600$ psia. The present generation of nuclear rockets can heat the hydrogen propulsive fluid to no more than 5000^o R, and dissociation is unimportant at this temperature. However, the effect of dissociation on the hydrogen propellant does become important at reactor operating temperatures approaching $10{,}000^o$ F, and such temperatures are definitely feasible in the case of the vortex-contained gas-phase reactors now being studied.

Calculations assuming uncatalyzed flow utilized a value of the dimensionless rate constant, C. The formula for C in algebraic and numeric form is as follows:

$$C = k_{r_R} \left(\frac{\bar{T}_d}{\bar{T}_R}\right)^{-s} \frac{\bar{\rho}_d^{\,2}}{m^2} \frac{\sqrt{\bar{A}^*}}{\sqrt{\frac{D}{2m}}}$$

$$= \frac{10^{15} \text{ cm}^6/(\text{mole}^2\text{sec}) \cdot (1/\bar{T}_R)^{-0} (1.90 \text{ g/cm}^3)^2 (30.48 \text{ cm})}{(1.008 \text{ g/mole})^2 \, (1.47 \cdot 10^6 \text{ cm/sec})}$$

$$= 0.7366 \; (10^{11})$$

Calculations assuming catalyzed flow required a value for the dimensionless rate constant, C_c, in addition to that for C. The formula for C_c in algebraic and numeric form is as follows:

$$C_c = 4\hat{A}\left(\frac{C_c}{M_c}\right)\left(\frac{\bar{T}_d}{\bar{T}_{R_c}}\right)^{\frac{1}{2}} \bar{\rho}_d \frac{\sqrt{\bar{A}^*}}{\sqrt{\frac{D}{2m}}}$$

$$= \frac{4 \left[2.7(10^{-13}) \text{ cm}^3/(\text{mole sec})\right] (.01) \cdot (175.8)^{\frac{1}{2}} \cdot [1.90 \text{ g/cm}^3] \cdot (30.48 \text{ cm})}{(28.0 \text{ g/mole}) \; (1.47 \cdot 10^6 \text{ cm/sec})}$$

$$= .2014 \; (10^8)$$

The ratio of catalyst activation energy to the dissociation energy for hydrogen is also required for catalyzed flow. The value assigned to this ratio in the present investigation is

$$E/D = \frac{4.2 \text{ kcal/mole}}{104.178 \text{ kcal/mole}} = .403 \; (10^{-1})$$

The properties assigned to the catalyst and appearing in the determination of C_c and E/D above are the low-temperature properties of ethylene as reported by Girouard.[5] Certainly ethylene cannot serve as a catalyst for the reassociation of hydrogen atoms under the conditions considered here. As yet, no similar study of possible catalysts for this reaction under high-temperature conditions appears to have been made. The use of these low temperature data thus represents only a hope that a catalyst may be found which possesses a potency at high-temperature equal to that of ethylene at low temperature.

The values of $\rho^* v^*$ applying to uncatalyzed and catalyzed flow through the nozzles are presented in Figs. 7 and 8a, respectively.

The solutions presented here for both optimum and comparison nozzles were obtained by numerical integration using a fourth-order Runge-Kutta method [10]. A suitably programmed digital computer of moderate size was employed in the actual calculations.

The Results

Fig. 7 shows the optimum nozzle contour obtained for the uncatalyzed flow of the model gas. The contours of two comparison hyperbolic nozzles are also included in this figure. Since results obtained for the uncatalyzed flows are so similar to the results obtained for the catalyzed flows except for the dimensionless position downstream of the throat at which a particular dimensionless area is achieved, further discussion of the uncatalyzed flows will be deferred until the catalyzed flows have been considered in detail.

Fig. 8 shows the optimum nozzle contour obtained for the catalyzed flow of the model gas. The contours of three comparison hyperbolic nozzles are also included in this figure. The flow conditions were calculated to a dimensionless area of at least 100 and a dimensionless static pressure of

no more than 10^{-8}. A minimum earth-orbital altitude of approximately one hundred kilometers was assumed as reasonable for any vehicle powered by a rocket engine of the type discussed here. At this altitude, the ambient pressure is approximately $3(10^{-4})$ Torr. or, in the dimensionless form used here, 10^{-8}.

The dimensionless length at which the static pressure in the comparison nozzle is equal to the static pressure in the optimum nozzle was determined for each comparison nozzle. The very small ticks near the intersections of the A vs. ζ curves in Fig. 8a indicate the value of ζ at which the static pressure has a common value (this static pressure is also noted near each intersection) for the gas within the optimum nozzle and one or the other of the comparison nozzles. A dashed line corresponding to the $A\{\zeta\}$ at which the static pressure of the gas in some one hyperbolic nozzle will be equal to 10^{-8} is also indicated in the figure.

Fig. 8b presents the velocity of the flowing gas at a particular location ζ. Since the optimum nozzle is only optimum if the ambient pressure is equal to the static pressure at any exit plane, this graph can also be interpreted as a presentation of optimum specific impulse versus ζ.

When Fig. 8b is considered in conjunction with Fig. 8a, it is apparent that no distinguishable difference between balanced pressure specific impulse of the optimum nozzle and a particular hyperbolic nozzle occurs when the exit static pressure of the optimum nozzle, the exit static pressure of the particular hyperbolic nozzle, and the ambient pressure are identical. A close check of the numerical results indicates that the specific impulse of the optimum nozzle is, at best, only a few tenths of one percent better than that of the comparison nozzle under these conditions.

Certainly this slight advantage could be obliterated by considerations of nozzle weight and frictional effects.

The curves CO and CH present specific impulse for optimum and hyperbolic nozzles extended beyond the balanced pressure point and yet exhausting to an ambient atmosphere whose pressure corresponds to that existing at $\zeta = \zeta_c$. Because of the greater divergence of the hyperbolic nozzle, the penalty in reduced specific impulse for extending the optimum and hyperbolic nozzles by equal length amounts is clearly greater for the hyperbolic nozzle. Nevertheless, for any length ζ, there is some hyperbolic nozzle whose balanced pressure specific impulse is virtually equal to that of the optimum nozzle of the same length. The curves BO and BH are off-design specific impulse curves relative to an ambient atmosphere for which the dimensionless static pressure is that corresponding to balanced pressure conditions where $\zeta = \zeta_{cB}$, viz., $p = 6.50\ (10^{-8})$.

A further investigation of equilibrium flow through the optimum nozzle contour showed that the equilibrium specific impulse was virtually equal to the optimum for finite chemical reaction rate.

Fig. 8c presents the mass fraction dissociated as a function of dimensionless distance downstream from the nozzle throat for (1) the two longest comparison nozzles and the optimum nozzle where the previously specified, catalyzed, finite-rate chemical reaction is assumed, and (2) the optimum nozzle contour where complete chemical equilibrium is assumed. It should now be recalled that α as well as specific impulse and thrust have been extremized by the variational methods employed here. And in the case of α, the optimum nozzle does provide a clearly lower value of α in the flowing gas at a given location, ζ, than the best hyperbolic

contour which might be selected. The value of C_C which can be realized by assuming equilibrium flow through the optimum nozzle is obviously somewhat below that which has been realized by the optimum nozzle finite-rate chemically reacting flow.

A Comparison of Results

As indicated previously, the analysis of uncatalyzed nozzle flow differed strongly from that of catalyzed nozzle flow only in the dimensionless length at which static pressure is equal to ambient pressure. In the case of operation at a dimensionless ambient pressure of 10^{-8}, both the uncatalyzed and catalyzed nozzles allow a dimensional balanced-pressure specific impulse of 1628 seconds. But the optimum nozzle for the expansion of the uncatalyzed gas to this ambient pressure is 84.24 meters long, while the optimum nozzle for the expansion of the catalyzed gas to this ambient pressure is 1.18 meters long.

Conclusions

From results obtained in the investigation reported here, it is concluded that very little increase in specific impulse can be obtained by optimizing the nozzle contour of a nuclear rocket which employs a vortex-contained gas-phase reactor to heat a gaseous hydrogen propulsive medium.

By contrast, although no improvement in specific impulse can be achieved by this means, the utilization of a potent catalyst to promote recombination of the hydrogen atoms before the gas leaves the rocket nozzle will allow a great reduction in nozzle length and weight for balanced-pressure exhaust to the same ambient pressure.

References

1. Lighthill, M. J., Dynamics of a Dissociating Gas, Part I, Equilibrium Flow, Journal of Fluid Mechanics, vol. 2, part I, pp. 1-32 (January, 1957).

2. Bray, K. N. C., Atomic Recombination in a Hypersonic Wind-Tunnel Nozzle, Journal of Fluid Mechanics, vol. 6, pp. 1-32 (October, 1958).

3. Clarke, J. F., The Flow of Chemically Reacting Gas Mixtures, C. O. A. Report No. 117, The College of Aeronautics, Cranfield, England (November, 1958).

4. Berns, R. R., Optimum Nozzle Contours for a Dissociating Gas with a Catalyst, Ph.D. Dissertation, Department of Mechanical Engineering, Kansas State University, Manhattan, Kansas (1966).

5. Girouard, H., Catalysis of Nozzle Flows, AIAA Preprint No. 64-98, Presented at the Aerospace Sciences Meeting, New York, New York, (January, 1964).

6. Kelley, H. J., An Investigation of Optimal Zoom Climb Techniques, IAS Report No. 59-16, Presented at the I.A.S. 27th Annual Meeting, New York, New York, January 26-29, 1959.

7. Krascella, N. L., Tables of the Composition, Opacity, and Thermodynamic Properties of Hydrogen at High Temperatures, NASA SP-3005, iii + 185 pps, 8 figures, (1963).

8. Kubin, R. F. and Presley, L. L., Thermodynamic Properties and Mollier Chart for Hydrogen from 300°K to 20,000°K, NASA SP-3002, 63 pps, 2 figures, 3 tables (1964).

9. Fowler, R. G., A Theoretical Study of the Hydrogen-Air Reaction For Application to the Field of Supersonic Combustion, Proceedings of the 1962 Heat Transfer and Fluid Mechanics Institute, Held at University of Washington, June 13-15, 1962, Stanford University Press, pp. 279-294.

10. Hildebrand, F. B., Introduction to Numerical Analysis, McGraw-Hill Book Co., Inc. (1956).

LIGHTHILL'S IDEALIZED DISSOCIATING DIATOMIC GAS

APPROXIMATIONS:

1. VIBRATIONAL EXCITATION IS NEGLIGIBLE.
2. IONIZATION IS NEGLIGIBLE.
3. THE CHARACTERISTIC DISSOCIATION DENSITY, $\bar{\rho}_d$, IS CONSTANT OVER THE RANGES OF PRESSURE AND TEMPERATURE WHICH ARE OF INTEREST WHEN DISSOCIATION IS A DOMINANT CONSIDERATION.
4. $$\frac{\bar{u} - \frac{D}{2m}\cdot\alpha}{\frac{k}{m}\bar{T}} = \frac{3}{2}$$

BY THESE ASSUMPTIONS, LIGHTHILL'S MODEL CAN BE DESCRIBED BY RELATIVELY SIMPLE ANALYTIC EXPRESSIONS:

$$\bar{p} = (1+\alpha)\frac{k}{2m}\bar{\rho}\bar{T},$$

$$\alpha_e^2/(1-\alpha_e) = (\bar{\rho}_d/\bar{\rho}_0)\cdot\exp\{-D/k\bar{T}\},$$

AND $$\bar{u} = \frac{3}{2}\frac{k}{m}\bar{T} + \frac{D}{2m}\cdot\alpha.$$

FIGURE 1.

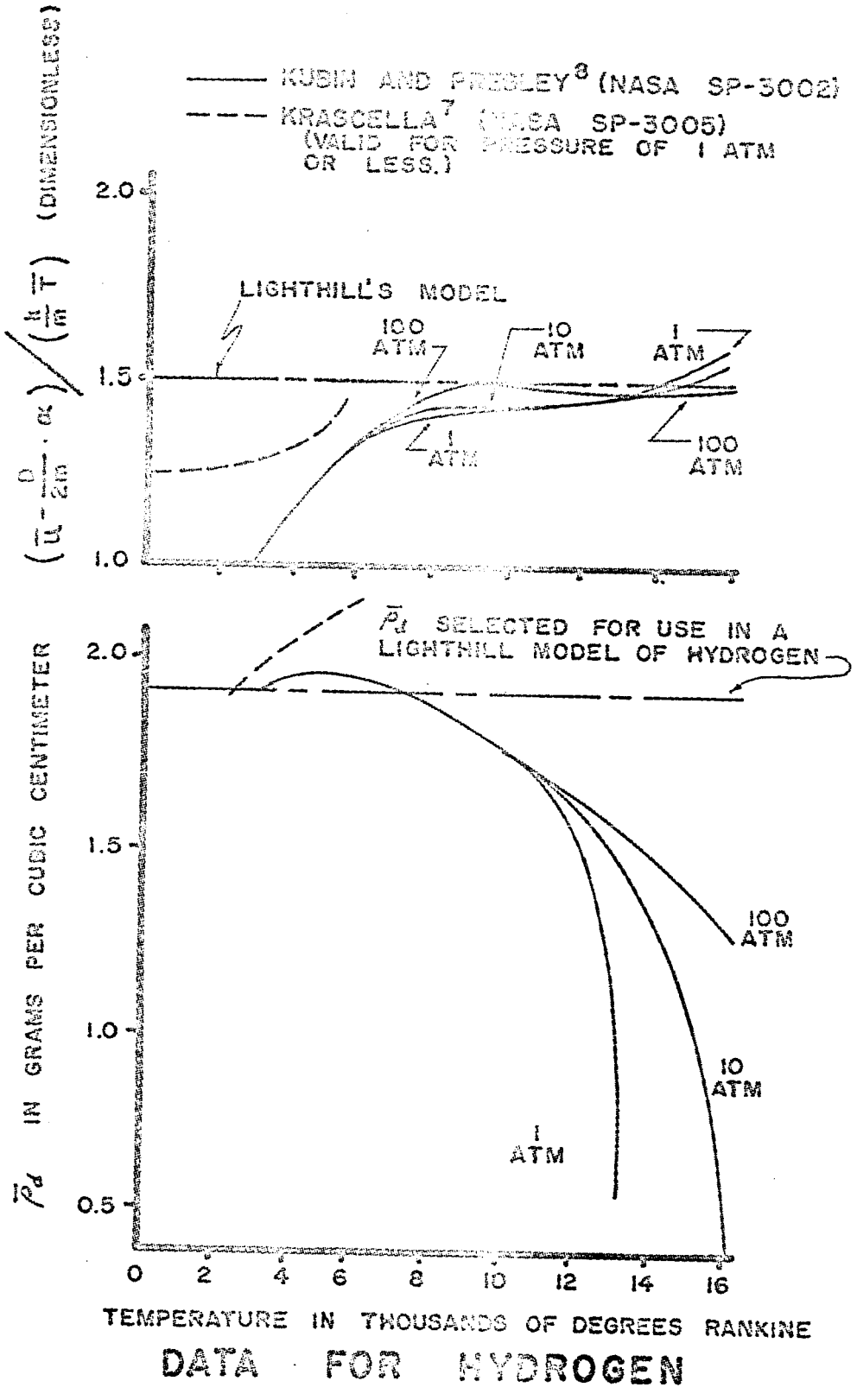

DATA FOR HYDROGEN

DRAY'S EQUATIONS

THE FLOW EQUATION:

$$f = Q i' + R \alpha' + \frac{i-\alpha}{A} A' = 0$$

WHERE

$$Q = \frac{3}{1+\alpha} - \frac{i-\alpha}{2(i_s - i)}$$

AND

$$R = 1 - \frac{3}{(1+\alpha)} \left(\frac{i-\alpha}{4+\alpha} \right)$$

THE REACTION RATE EQUATION:

$$g = \alpha' - \Gamma = 0$$

WHERE

$$\Gamma = \frac{C(1+\alpha)\rho^* v^*}{2(i_s - i)A} \left\{ (1-\alpha) C^{-\frac{1}{T}} - \frac{\rho^* v^*}{A\sqrt{2(i_s - i)}} \alpha'^2 \right\}$$

$$+ \frac{C_0 e^{-E/(RT)} T^{\frac{1}{2}}}{\sqrt{2(i_s - i)}(1+\alpha)} \left\{ (1-\alpha) C^{\frac{1}{T}} - \frac{\rho^* v^*}{A\sqrt{2(i_s - i)}} \alpha'^2 \right\}$$

THE AREA DISTRIBUTION:

$$A = A(\xi)$$

FIGURE 3.

PROPELLANT SPECIFIC IMPULSE

$$I_{SP} = \sqrt{2(i_o - i)} + \frac{(1+\alpha)\left(\frac{i-\alpha}{4+\alpha}\right)}{\sqrt{2(i_o - i)}} - \frac{P_a A}{\rho^* v^*}$$

OR, IN DIFFERENTIAL FORM,

$$I'_{SP} = \frac{1+\alpha}{(4+\alpha)\sqrt{2(i_o - i)}} \frac{i-\alpha}{A} A' - \frac{P_a}{\rho^* v^*} A'$$

$$= \frac{p - P_a}{\rho^* v^*} A'$$

FOR CONVENIENCE, LET

$$\Theta = I'_{SP}$$

FIGURE 4.

FORMULATION OF THE VARIATIONAL PROBLEM

LAGRANGE FUNCTION:

$$F = -e + \lambda f + \mu g$$

WHERE λ AND μ ARE LAGRANGIAN MULTIPLIERS.

EULER EQUATIONS:

$$F_\alpha - \frac{d}{d\xi}(F_{\alpha'}) = 0$$

$$F_i - \frac{d}{d\xi}(F_{i'}) = 0$$

$$F_A - \frac{d}{d\xi}(F_{A'}) = 0$$

NATURAL END CONDITION:

$$p_a = p$$

FIGURE 5.

THE BOUNDARY VALUE PROBLEM

CONSTANTS:

C = UNCATALYZED REACTION RATE.

C_c = CATALYZED REACTION RATE.

$E/D = \dfrac{\text{CATALYST ACTIVATION ENERGY}}{\text{HYDROGEN DISSOCIATION ENERGY}}$

i_o = STAGNATION SPECIFIC ENTHALPY.

$\rho^* v^*$ = MASS FLUX DENSITY AT THE THROAT.

INITIAL CONDITIONS:

i, α, AND A.

EQUATIONS:

$$i' = \frac{\Gamma\lambda - (i-\alpha)\Gamma\lambda_\alpha + R\Gamma A\lambda_A - A\Gamma_A/\Gamma}{\lambda + (i-\alpha)\lambda_i - QA\lambda_A}$$

$$\alpha' = \Gamma\{i, \alpha, A\}$$

$$A' = -\frac{(Q+R)\Gamma\lambda + (i-\alpha)\Gamma(R\lambda_i - Q\lambda_\alpha) - QA\Gamma_A/\Gamma}{[(i-\alpha)/A]\{\lambda + (i-\alpha)\lambda_i - QA\lambda_A\}}$$

where $$\lambda = \frac{QA\Gamma_A - (i-\alpha)\Gamma_i}{[(q+\alpha)/(1+\alpha)]R\Gamma^2}$$

Figure 6

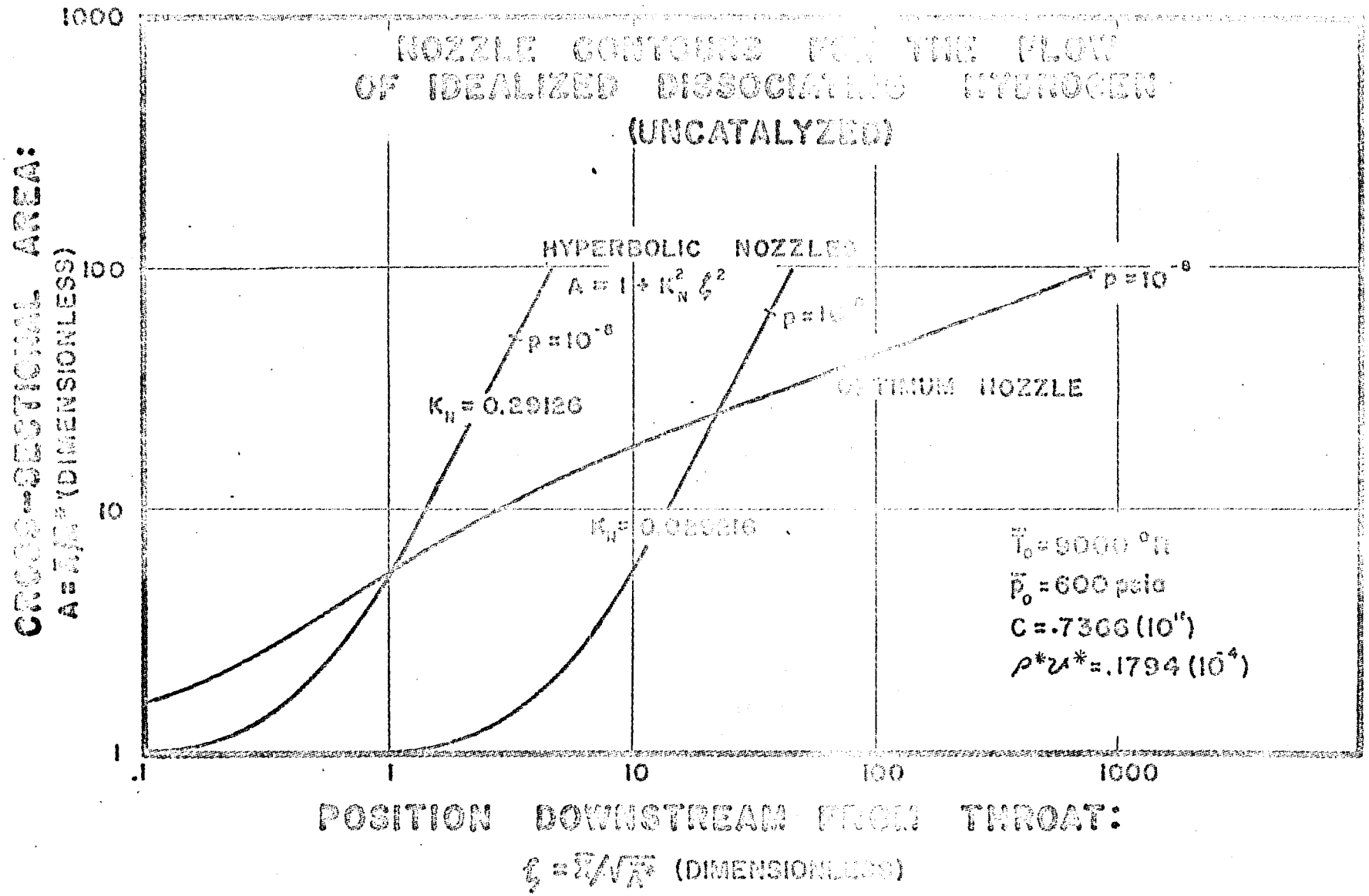
NOZZLE CONTOURS FOR THE FLOW
OF IDEALIZED DISSOCIATING HYDROGEN
(UNCATALYZED)
HYPERBOLIC NOZZLES
$A = 1 + K_N^2 \xi^2$
$p = 10^{-6}$
$K_N = 0.29126$
OPTIMUM NOZZLE
$\bar{T}_0 = 9000\ ^\circ R$
$\bar{p}_0 = 600\ psia$
$C = .7306\ (10^{11})$
$\rho^* u^* = .1794\ (10^4)$
CROSS-SECTIONAL AREA:
$A = \bar{A}/\bar{A}^*$ (DIMENSIONLESS)
1000
100
10
1
.1
1
10
100
1000
POSITION DOWNSTREAM FROM THROAT:
$\xi = \bar{x}/\sqrt{\bar{A}^*}$ (DIMENSIONLESS)

FIGURE 7.

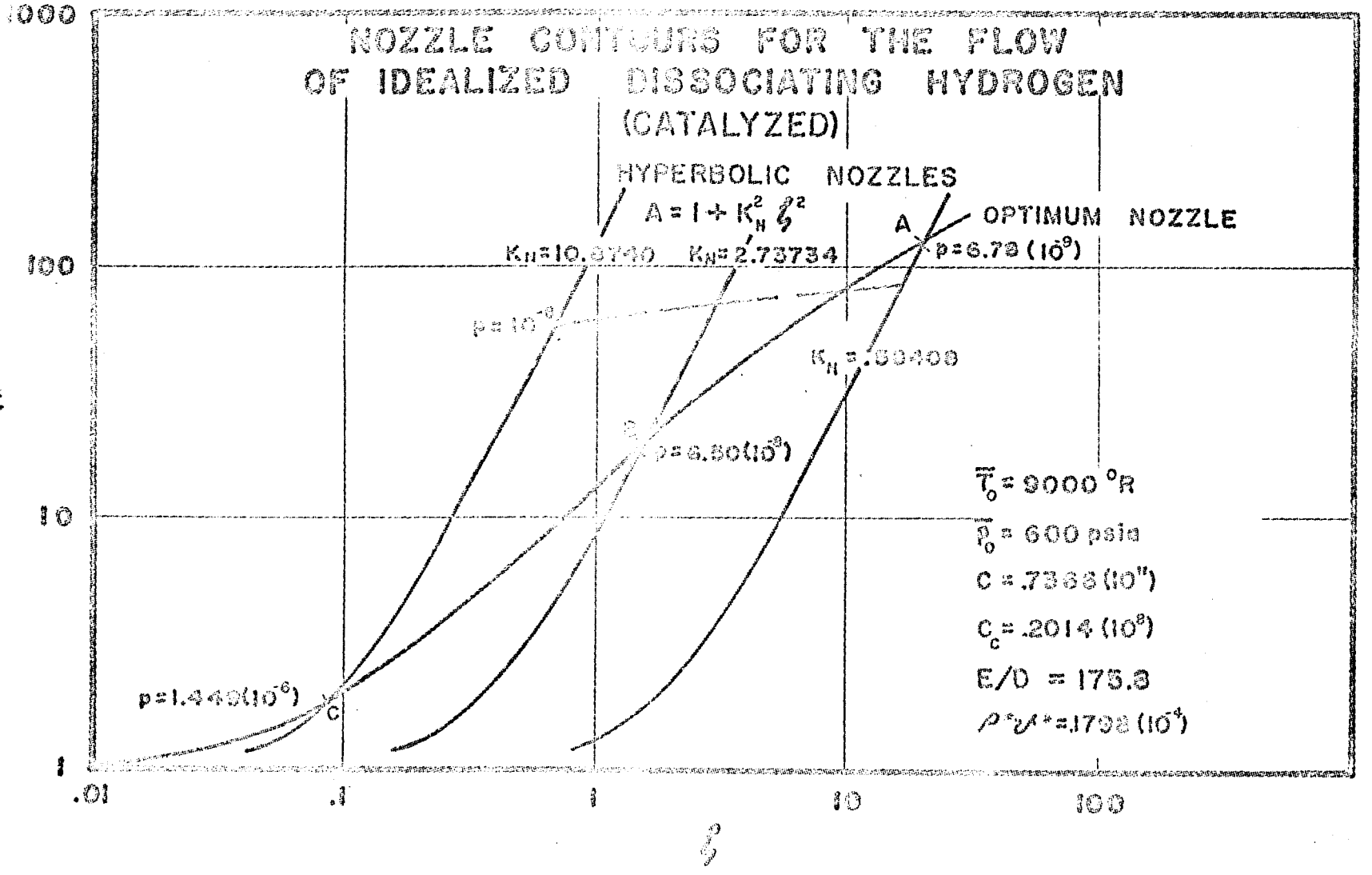
NOZZLE CONTOURS FOR THE FLOW
OF IDEALIZED DISSOCIATING HYDROGEN
(CATALYZED)
HYPERBOLIC NOZZLES
$A = 1 + K_N^2 \xi^2$
OPTIMUM NOZZLE
K_N=10.87490
K_N=2.73734
K_N=.50408
p=6.78 (10⁹)
p=10⁹
p=6.80(10⁸)
p=1.440(10⁶)
A
B
C
$\bar{T}_o$ = 9000 °R
$\bar{p}_o$ = 600 psia
C = .7388 (10⁻⁴)
C_c = .2014 (10⁻⁸)
E/D = 175.3
$\rho^* u^*$ = .1798 (10⁻⁴)
1000
100
10
1
.01
.1
1
10
100
A
ξ

FIGURE 6a

GAS VELOCITY VS. NOZZLE LENGTH
FOR THE NOZZLES OF FIG. 6a

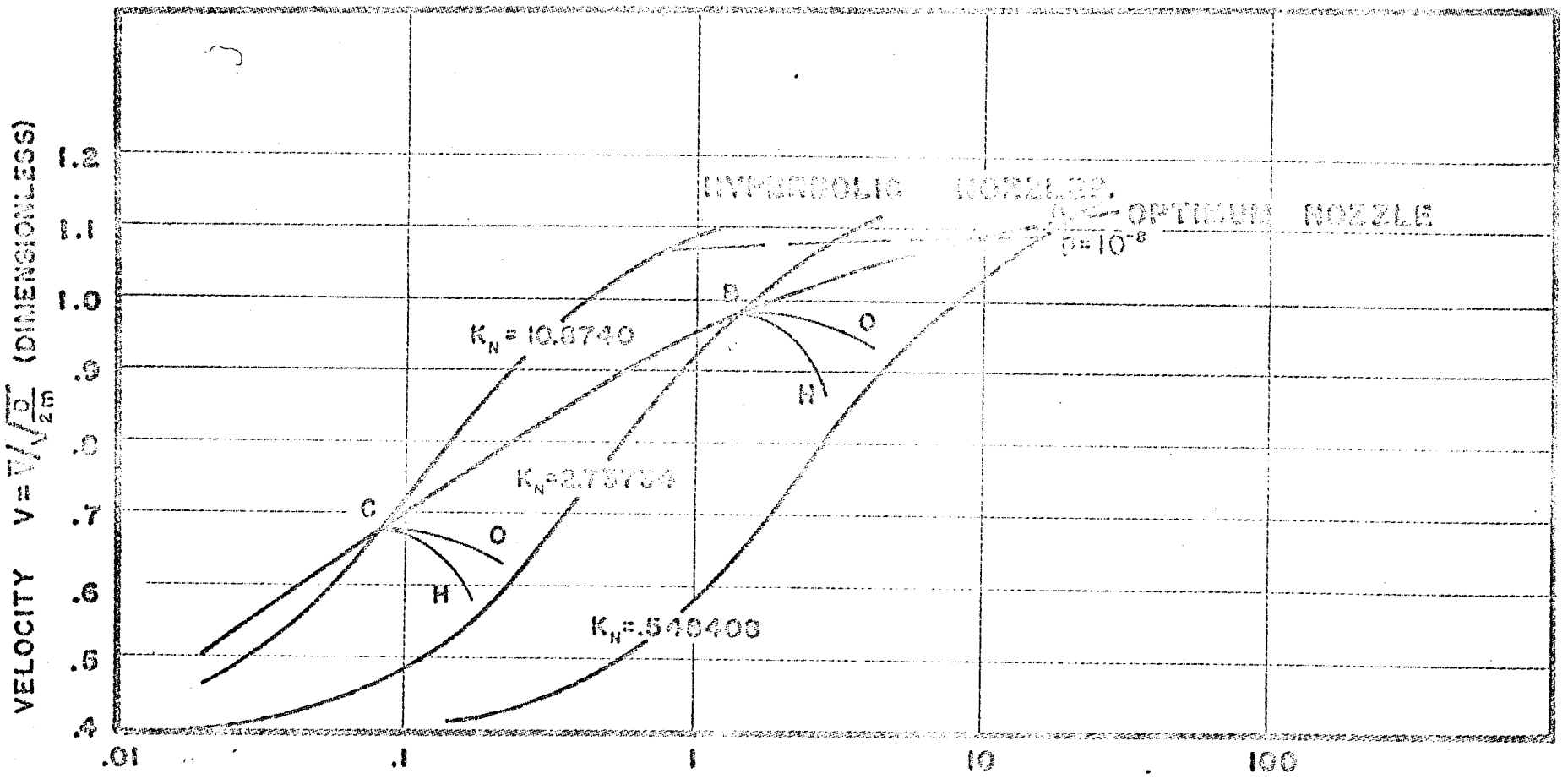

FIGURE 6b

MASS FRACTION DISSOCIATED, α (DIMENSIONLESS)

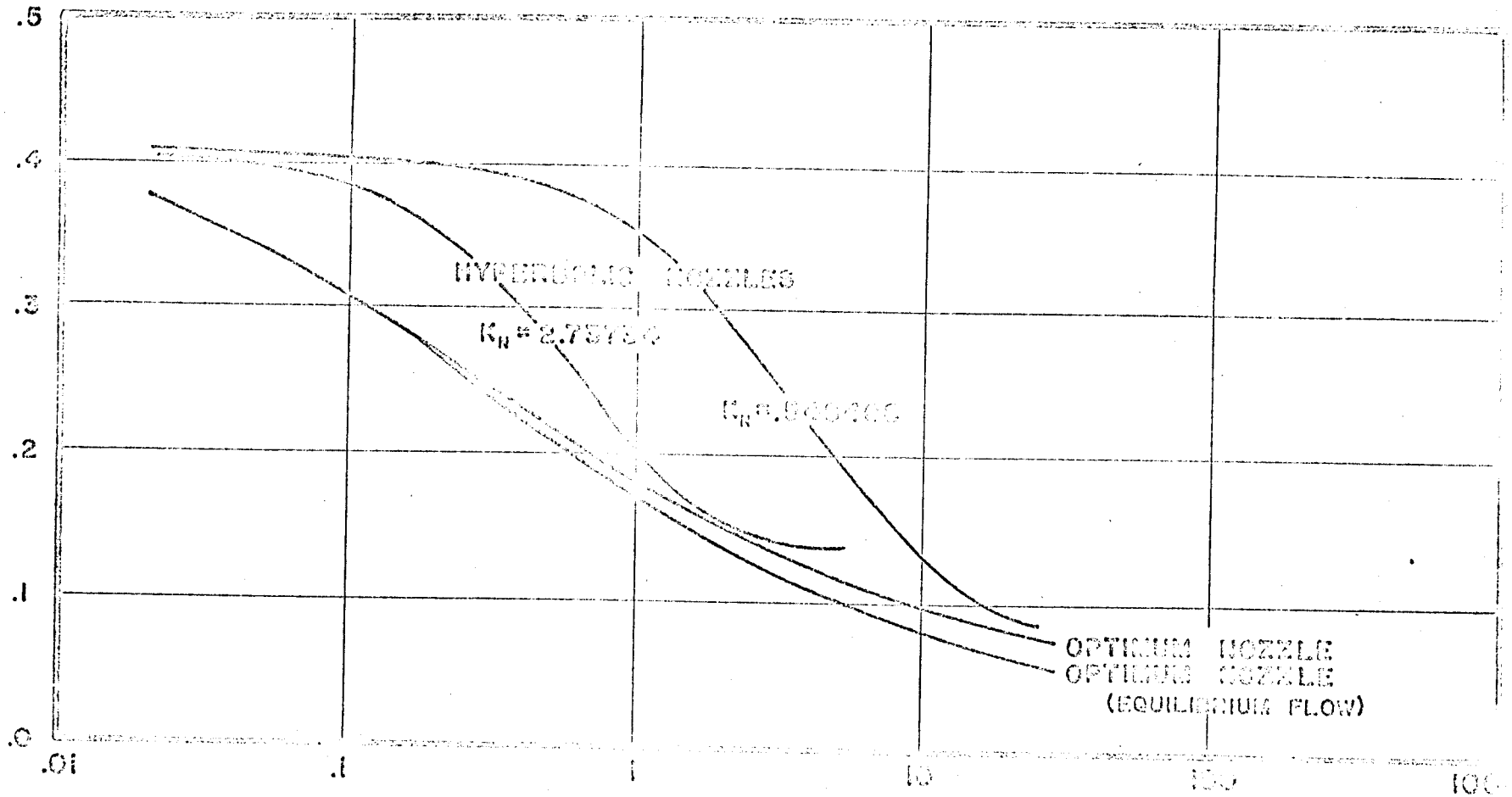

FIGURE 6c